Use of Nanostructured Photocatalysts for Dye Degradation: A Review

Victor Ruiz-Santoyo[1*], Beatriz A. Andrade-Espinoza[2], Rafael Romero-Toledo[1,3],
Luis M. Anaya-Esparza[4], Zuamí Villagrán[5], Antonio Guerra-Contreras[6]

[1] Engineering Department, Division of Agricultural Sciences and Engineering, University Center of Los Altos, University of Guadalajara, Av. Rafael Casillas Aceves 1200, 47600 Tepatitlán de Morelos, Mexico
[2] Department of Clinics, Division of Biomedical Sciences, University Center of Los Altos, University of Guadalajara, Av. Rafael Casillas Aceves 1200, 47600 Tepatitlán de Morelos, Mexico
[3] Chemical Engineering Department, Division of Natural and Exact Sciences, University of Guanajuato, Lascuráin de Retana No. 5, 36000 Guanajuato, Mexico
[4] Department of Livestock and Agricultural Sciences, Division of Agricultural Sciences and Engineering, University Center of Los Altos, University of Guadalajara, Av. Rafael Casillas Aceves 1200, 47600 Tepatitlán de Morelos, Mexico
[5] Department of Health Sciences, Division of Biomedical Sciences, University Center of Los Altos, University of Guadalajara, Av. Rafael Casillas Aceves 1200, 47600 Tepatitlán de Morelos, Mexico
[6] Department of Chemistry, Division of Natural and Exact Sciences, University of Guanajuato, Lascuráin de Retana No. 5, 36000 Guanajuato, Mexico
* Corresponding author, e-mail: victor.ruiz8959@alumnos.udg.mx

Abstract

Among the technologies proposed for wastewater treatment, the Advanced Oxidation Processes are viable and technological strategies for dyes degradation. Different photocatalytic systems classified in metal oxides alone or combined through hybrid composites or immobilized onto supports have been designed in various nanostructured shapes for their application in the photodegradation of polluting dyes. This review aims to describe the dyes as an environmental threat, photocatalysis as an effective process to remove dyes from water and provide an overview of the recent studies using photocatalytic systems grouped according to their development. Furthermore, this review describes the main parameters of a photocatalytic system with an important role in dye photodegradation. Finally, we discuss the limitations of photocatalysis for real industrial applications and the challenges for this environmental nanotechnology.

Keywords

advanced oxidation process, dyes, photocatalytic systems, water treatment

1 Introduction

The use of natural dye for textile dyeing has been practiced for 5,000 years ago. On the other hand, the discovery and application of synthetic dyes begun in the 19th century by displacing the use of natural dye. Nowadays, the global colorant market is about 32 billion USD and is projected to increase to around 42 billion USD by 2021 [1]. Synthetic dyes present advantages compared to natural dyes because of their lower prices, repeatability, and wide range of bright shades with considerably improved color fastness properties [2]. Dyes are colorful substances designed to give a hue to any colorable materials, and this is possible as dyes can attach themselves to any amenable materials. Moreover, dyes are composed of a group of atoms known

as chromophores, responsible for the dye color. Dyes are sorted according to their application and chemical structure and are classified as acid, basic, direct, mordant, and reactive dyes, which are examples of soluble dyes, whereas azo, disperse, sulphur and vat dyes are an example of insoluble dyes [3]. The azo dyes kind, molecules with one or more azo (N=N) bridges linking substituted aromatic structures, represent a 70% of the global production and are the most frequently utilized dyes [4]. Unfortunately, the dye industry dramatically contributes to global pollution, generating consequences to the ground and water due to its toxic, carcinogenic, and xenobiotic repercussions. On the other hand, researchers have proposed using the Advanced

Oxidation Processes (AOP's) as an attractive technology for removing a wide range of emerging contaminants. The AOP's involve the in-situ production of highly reactive oxygen species such as hydroxyl radicals (OH·) and superoxide anion radicals ($O_2^{·-}$) with oxidation potentials of 2.7 and −2.3 eV, respectively. These species can be initiated by primary oxidants (e.g., H_2O_2, O_3), energy sources (e.g., UV light, ultrasonic, and heat), or catalysts (e.g., TiO_2, ZnO, and ZrO_2) [5]. Among AOP's, photocatalysis is a viable alternative process to remove the emerging contaminants at standard temperature and pressure (STP) conditions by oxidation reactions. As mentioned, a huge variety of nanomaterials with photocatalytic activities have been used in environmental remediation because they propose using solar energy to promote photoreaction, making the process cheaper and environmentally friendly. Moreover, the favorable combination of electronic structure, light absorption properties, charge transport characteristics, improved textural proprieties, excited lifetimes, and versatility in shapes and sizes of metal oxides has made them possible for their application in photocatalysts [6]. Therefore, this review compiles the information of current photocatalytic systems based on mixed oxide nanoparticles used to degrade water dyes. In addition, scientific aspects were discussed, some social concerns and current trends of photocatalysis are also described.

2 Dyes and their environmental impact

Nowadays, it is estimated that 700,000 tons of various colouring from about 100,000 commercially accessible dyes are manufactured each year [7]. Nevertheless, between 10% and 15% of the synthetic dyes are lost during different textile industries processes [4]. Moreover, about 40,000–50,000 tons of dyes are discharged in water bodies from natural or anthropogenic means [8]. The azo dyes are considered one of the most difficult compounds to be removed and degraded from aqueous systems; thereby, the public demand for color-free discharge has rendered decolorization of wastewater is a priority [9]. During the dyeing processes, not all dyes that are applied to the fabrics are fixed on them, and usually, a portion of these dyes that remains unfixed to the fabrics and gets washed out, this amount of generated textile wastewater can reach more than 300 L kg^{-1} of product [10]. These unfixed dyes are found to be in high concentrations in textile effluents, and the composition of the wastewater will depend on the different organic-based compounds and the dyes used in the dry and wet-processing steps. Moreover, textile wastewaters can generate fluctuations in parameters such as chemical oxygen demand (COD), total organic carbon (TOC), biochemical oxygen demand (BOD), pH, flavor, colour, and odor when are released in aquifers [11]. The releasing of dye effluents into aquifers is undesirable due to the high impact on photosynthesis of aquatic organisms, and the carcinogenic nature and mutagenicity of many of these dyes and their breakdown products [11]. One of the main concerns is reducing the penetration of light when dyes are dissolved in water, which can cause an alteration of the photosynthetic activity and thus modify the natural balance of flora and fauna. Furthermore, these effluents can pass through soil layers and may contaminate nearby surface and underground water. For human health affectations, the dermal exposure of the dye precursors leads to bladder cancer, since as dyes contain aromatic amines, they can generate damage in the DNA of cells, leading to the risk of cancer disease. Moreover, dyes can promote other human health problems such as allergies, urticaria, angioedema, hyperactivity, ocular irritability, aggressiveness and learning impairment related to intake of dye [12].

3 Photocatalysis

Photocatalysis was proposed in 1972 by Fujishima and Honda [13]; they discovered that TiO_2 decomposes water into hydrogen and oxygen under light irradiation. In this context, photocatalysis is the acceleration of a reaction using a catalyst in light presence with an adequate wavelength. To carry out a photocatalytic process, the incident light on the catalyst should supply energy equal to or greater than the semiconductor band gap value (eV). This energy can be calculated using Eq. (1):

$$Eg\,(\text{eV}) = 1239.9/(\lambda\,(\text{nm})), \tag{1}$$

where λ is the wavelength value, for example, if a semiconductor has a band gap of 3.0 eV, the incident wavelength value on photocatalyst should be equal to or under 413.3 nm to photo-excite the electrons from the valence band (V_B) to the conduction band (C_B). Therefore, an electron belonging to V_B is excited to the C_B, giving as a result a pair of species, a hole (h^+) in the V_B and an electron (e^-) in the C_B [14], Fig. 1 and Eq. (2). The recombination of e^- and h^+ carriers must be prevented to promote the photocatalytic reaction. The excited electrons that are now in C_B (e_{CB}^-) react with oxygen (O_2) to produce superoxide radicals ($O_2^{·-}$) which degrade pollutants in water (H_2O) and carbon dioxide (CO_2), Eqs. (3) and (4). On the other hand, the water oxidation reaction takes place in the
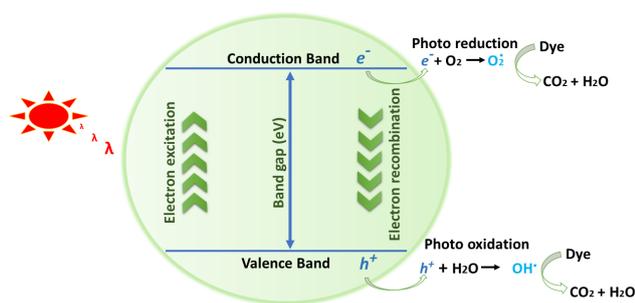
Fig. 1 Photocatalysis general mechanism

positive hole in valance balance (h_{VB}^+) generating hydroxyl radicals (OH˙) and hydrogen ions (H⁺) to degrade pollutants in water (H_2O) and carbon dioxide (CO_2) as well, Eqs. (5) and (6) [15]. In a typical photocatalysis process, two different reactions occur; an oxidation reaction due to photo-induced positive holes and a reduction reaction due to photo-induced negative electrons [16]. Furthermore, the oxidation potentials of hydroxyl (OH˙) and superoxide radical ($O_2^{\cdot-}$) are 2.7 and −2.3 eV respectively, whereas the oxidation potential of organic molecules ranged from −1 to 2 eV but, due to the difference in potential between the reactive oxygen species and the pollutant molecules, an organic pollutant molecule in contact with the hydroxyl (OH˙) or superoxide radical ($O_2^{\cdot-}$) will either gain or lose electrons immediately through chain reactions resulting in the mineralization of the organic molecules forming CO_2 and H_2O as innocuous products.

$$catalyst + h\nu \rightarrow e_{CB}^- + h_{VB}^+ \left(excitation\right) \tag{2}$$

$$O_2 + e_{CB}^- \rightarrow O_2^{\cdot-} \left(O_2 \; reduction\right) \tag{3}$$

$$O_2^{\cdot-} + pollutant \rightarrow H_2O + CO_2 \tag{4}$$

$$H_2O + h_{VB}^+ \rightarrow OH^{\cdot} + H^+ \left(OH^- \; oxidation\right) \tag{5}$$

$$OH^{\cdot} + pollutant \rightarrow H_2O + CO_2 \tag{6}$$
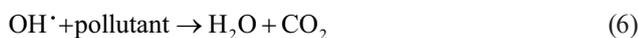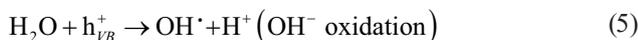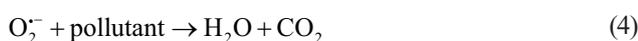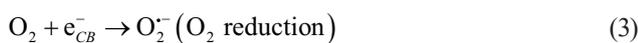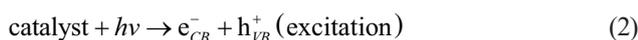
The most important characteristics of a photocatalytic system are the morphology, high surface area, thermal and mechanical stability, reusability, active sites, and desired band gap [17]. According to Molinari et al. [18], photocatalysis offers some advantages:

1. It avoids the application of hazardous heavy metal compounds and oxidants/reducing agents.
2. It permits the mineralization of the pollutants with the generation of safer by-products as H_2O and CO_2.
3. It is an alternative to traditional high energy-demanding treatment methods by using solar energy as the energy source.
4. It degrades a moderate range of pollutant concentrations.
5. It can be combined with another wastewater method to get a better water quality

Additionally, the use of photocatalysis at industrial processes is still restricted due to the recombination of the photo-generated e⁻ and h⁺ carriers, which releases energy in unproductive heat form, fast-backward reaction, and the inability to utilize solar radiation energy since around 5% of solar radiation is UV light [19].

3.1 Photocatalysts synthesis methods

Nanotechnology is defined as the ability to structure matter in atomic and molecular levels between 1–100 nm [20]. At this scale, materials have novel size-dependent features different from their larger counterparts. Nanomaterials have been developed in several forms, such as nanotubes, nanowires, flakes, particles, rods, films, quantum dots, and colloids [21]. Nanotechnology has opened a wide possibility field for designing nanomaterials with the objective application through manipulating synthesis conditions, which allows us to design nanostructures with attractive features in shape, size, mechanic resistance, and chemistry activity [22]. The synthesis of nanomaterials with a defined morphology is an important key to getting nanostructures with desired chemical and physical properties. Moreover, the chemical activity depends not only on their size, shape, morphology, and phase composition, as well as the synthesis route [23]. This favors the preparation of nanostructured materials with desirable features, which enhance the catalytic activity of the photocatalyst. Furthermore, the power of the lamp also plays an important role with influence on the performance of the photocatalyst. Several nanoparticles synthesis methods have been reported, and each one is selected depending on the nanostructures application. The most common methods for photocatalysts synthesis are colloidal, microwave radiation, sol-gel, hydrothermal, chemical vapor deposition, photochemistry reduction, solvothermal, electrochemical deposition process, and electrospinning [24]. Among these methods, the sol-gel is the most attractive way to synthesize photocatalysts due to low cost, reproducibility, high purity, synthesis time, variable control, low process

temperature, and homogeneity in particle size [25, 26]. The sol-gel method for preparing metal oxide photocatalysts relies on the hydrolysis and polycondensation of the metal alkoxides used as precursors, $M(OR)_x$ (M = Si, Ti, Zr, Zn, Al, Sn and Mo) to react in aqueous or organic phase.

4 Nanostructured photocatalytic systems for dye degradation

Throughout history, various photocatalytic systems have been developed to eliminate the dyes present in water. The development of photocatalytic materials through history can be divided into three groups: single component photocatalysts in suspension, heterojunction photocatalysts (multi-component in suspension), and immobilized photocatalysts, Fig. 2.

4.1 Single component photocatalysts

Elements such as TiO_2, ZnO, ZrO_2, Fe_2O_3, CdS, and ZnS are semiconductors and can act as sensitizers for light-induced redox processes due to the electronic structure of the metal atoms in chemical combination, which are characterized by an empty C_B and a filled V_B [27]. When these kinds of materials are irradiated with energy equal to or greater than its band gap value (eV), an e^- from V_B migrates to the C_B generating an h^+ behind. The h^+ may react either with electron donors in the solution or with hydroxide ions to produce powerful oxidizing species like superoxide radicals ($O_2^{\cdot-}$) and hydroxyl ($OH^{\cdot}$) radicals. Nevertheless, the recombination process of the e^- and h^+ carriers must be avoided to favor the photocatalysis reaction. TiO_2 was the first material used and investigated for the water-splitting reaction. Years later, its application increased to other fields like H_2 production, water, and air

pollutant oxidation, antibacterial activity, and solar cells development. However, due to its large band gap (3.2 eV for anatase and 3.0 eV for rutile), it only can operate under UV light irradiation. Indeed, the anatase phase of TiO_2 is preferred catalytic reactions due to its conferred features by its crystallinity nature [28]. In this context, other metal oxides with a wide use for photocatalytic purposes are ZnO and ZrO_2. The ZnO can present the crystalline phases type wurtzite, zinc blende, or rock salt. Moreover, the ZnO is seen as the substitute for TiO_2 and is considered as an efficient and promising candidate in environmental management systems because of its unique characteristics, such as direct and wide band gap in the near-UV spectral region, strong oxidation ability, suitable photocatalytic property, and a large free-exciton binding energy so that excitonic emission processes can persist at or even above room temperature [29]. For its part, the ZrO_2 can present the cubic, tetragonal, or monoclinic crystal structure (eV = 3.25–5.1 eV, depending on the preparation technique), and it belongs to the group of semiconductor materials. In this context, it has been reported that ZrO_2 can cause higher photocatalytic degradation than nano TiO_2 [30]. Moreover, the manipulation of ZrO_2 morphological tuning, porous structure control, and crystallinity development is required to enhance the light-harvesting capability, prolong the lifetime of photoinduced electron-hole pairs, and facilitate the reactant accessibility to surface active sites [31]. Fig. 3 shows the band gap of common semiconductors, while Table 1 [31–44] shows representative first group photocatalysts.

This first group of metal oxides including the TiO_2 [32–37], ZrO_2 [31, 38, 39], and ZnO [40–44] exhibited good physical features like thermal and mechanical
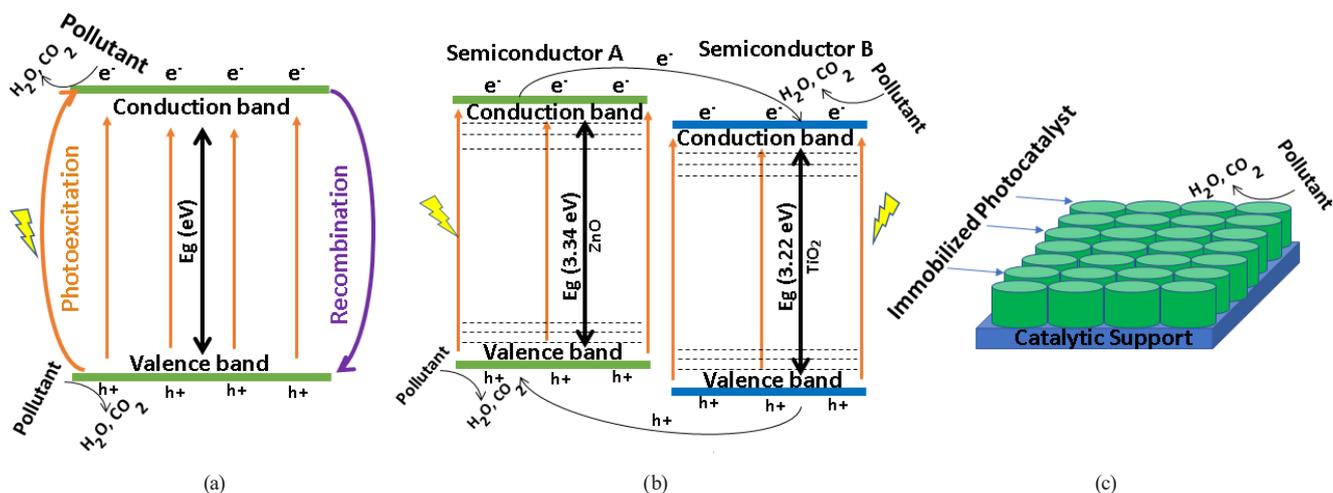

Fig. 2 Classification of the photocatalysts according to their development, (a) First group, (b) Second group, (c) Third group
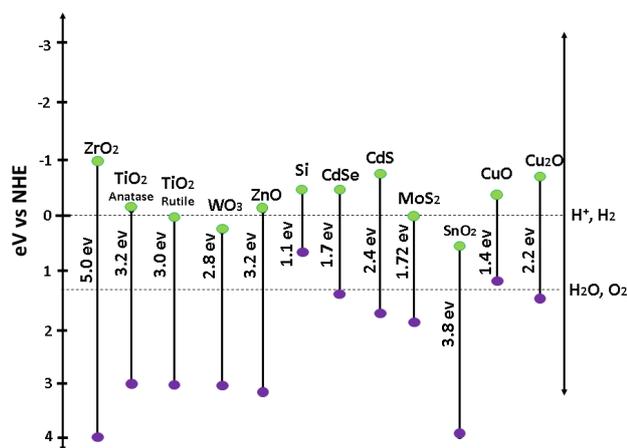
Fig. 3 Band gap of semiconductors (eV) versus Normal Hydrogen Electrode

stability, low toxicity and cost of production, reusability, and easy reactivation. However, their main drawback is their wide band gap value from 3 to 5 eV and the recombination process that present, by affecting the production of the e$^-$ and h$^+$ carriers. Therefore, a new group of photocatalysts with superior features of coupled nanomaterials was developed, which are based in heterojunctions.

4.2 Heterojunction photocatalysts

To enhance the visible light absorption efficiency of the photocatalyst, the electronic structure of the nanomaterial needs to be modified [45]. Methods such as doping, metal loading, and heterojunctions have been used to efficiently separate the photogenerated e$^-$ and h$^+$ carriers in

Table 1 TiO$_2$, ZrO$_2$ and ZnO applied for the dye removal

No	Photocatalyst	Synthesis Method	Morphology	Size (nm)	Band gap (eV)	Light	Dye	Time (min)	Degradation (%)	Ref.
1	TiO$_2$	Degussa P-25	-	30	3.0	UV	Methyl red	60	75	[32]
2	TiO$_2$	Degussa P-25	-	30	3.0	UV	Congo red	120	95	[32]
3	TiO$_2$	Degussa P-25	-	30	3.0	UV	Methyl blue	120	98	[32]
4	TiO$_2$	Hydrolysis of TiCl$_4$	Irregular	6.5	3.6	UV	Methylene blue	120	85	[33]
5	TiO$_2$	Hydrolysis of TiCl$_4$	Irregular	6.5	3.6	UV	Congo red	80	99.7	[33]
6	TiO$_2$ P-25	Hydrothermal	-	32	3.2	UV	Violet 26	60	93	[34]
7	TiO$_2$ P-25	Hydrothermal	Irregular	30	3.0	UV	Methylene blue	30	95	[35]
8	TiO$_2$ P-25	Hydrothermal	Irregular	30	3.0	UV	Methyl Orange	30	70	[35]
9	Core-shell structured TiO$_2$	One-step hydrogen treatment	Core-shell	30–40	3.0	Vis	Methylene blue	150	96	[36]
10	TiO$_2$	Hydrothermal	Cube	80–100	3.3	UV	Acetate Red X3B	30	98	[37]
11	ZrO$_2$	Electrochemical	-	-	-	UV	Methyl orange	60	80	[38]
12	ZrO$_2$	Electrochemical	-	-	-	UV	Methylene blue	60	92	[38]
13	ZrO$_2$	Electrochemical	-	-	-	UV	Congo red	60	87	[38]
14	ZrO$_2$	Electrochemical	-	-	-	UV	Malachite green	60	100	[38]
15	ZrO$_2$ monoclinic	Precipitation	Semiglobular	34	3.25	UV	Methyl Orange	110	99	[31]
16	ZrO$_2$ tetragonal	Precipitation	Semiglobular	17	3.58	UV	Methyl Orange	110	90	[31]
17	ZrO$_2$ cubic	Hydrothermal	Semiglobular	20	4.33	UV	Methyl Orange	110	80	[31]
18	ZrO$_2$-Zeolite	Sol-gel method and precipitation	Semispherical	40.8	-	UV	Methyl Orange	80	100	[39]
19	ZnO	Hydrothermal	-	-	3.3	UV	Violet 26	60	90.1	[34]
20	ZnO	Co-precipitation	Slit platelets	550	-	UV	Reactive Blue 19	360	100	[40]
21	ZnO	Co-precipitation	Slit platelets	550	-	UV	Reactive blue 21	360	91	[40]
22	ZnO	Ultrasonication	Semiglobular	17.5	3.25	Sunlight	Methylene blue	120	89.7	[41]
23	ZnO	Calcination	Irregular	10	-	UV	Malachite green	150	98.5	[42]
24	ZnO	Precipitation and ultrasound	Spherical	50	-	UV	Reactive blue 203	20	85.4	[43]
25	ZnO	Sol-gel	Rod-like	22–50	3.37	UV	Methyl orange	30	99.7	[44]
26	ZnO	Sol-gel	Rode-like	22–50	3.37	UV	Congo red	30	92.1	[44]
27	ZnO	Sol-gel	Rode-like	22–50	3.37	UV	Direct black 38	30	99.45	[44]

a photocatalytic semiconductor. The created electronic structure of the new photocatalyst could decrease the recombination of the carriers due to the creation of new energy levels by trapping the electrons by reducing the recombination of the charge carries (Fig. 4 (b)) [46]. A heterojunction is the creation of an interface between two different semiconductors with unequal band gap structure, resulting in band alignments. In this sense, different classes of heterojunctions have been reported:

1. semiconductor–semiconductor,
2. semiconductor–metal,
3. semiconductor–carbon, and
4. multicomponent heterojunction [47].

The principal requirement to create a heterojunction, is that semiconductors should exhibit dissimilar band gaps, and the narrow band gap must lie in the visible region. In addition, in the direct band gap, the highest energy level of the V_B aligns with the lowest energy level of the C_B to momentum [48], hence direct band gap is preferred over the indirect band gap. There are three types of conventional heterojunction photocatalysts, those with a straddling gap (type-I, Fig. 4 (a)), with a staggering gap (type-II, Fig. 4(b)), and with a broken gap (type-III, Fig. 4 (c)), [49, 50].

In the type-I heterojunction, the C_B and the V_B of semiconductor A are higher and lower than those corresponding of the semiconductor B. In other words, the band gap of one semiconductor B is insideof the band gap of the A semiconductor. When the photocatalyst is irradiated with the appropriate energy, the e⁻ and h⁺ carriers from semiconductor A migrate and are caught by the C_B and V_B of semiconductor B. Since e⁻ and h⁺ carriers are caught on the same semiconductor, the charge carriers cannot be effectively separated. In the type-II heterojunction, the C_B and the V_B levels of semiconductor A are higher than the corresponding C_B and V_B of semiconductor B. Therefore, under light irradiation, the photogenerated electrons from A will migrate to C_B of semiconductor B, while the photogenerated holes from semiconductor B will migrate to V_B of semiconductor A. In both cases, the redox ability will be also considerably reduced because the redox reaction occurs on semiconductor with the lowest redox potential. In the type-III heterojunction, the C_B and V_B of semiconductor A are higher than the C_B of semiconductor B, and the band gaps do not overlap. The carrier transfer is like type-II, just more pronounced. For this case, the e⁻ and h⁺ carriers migration and separation between the two semiconductors cannot be carried out, making it unsuitable for enhancing the separation of the e⁻ and h⁺ carriers [51]. From the three cases, the type-II heterojunction looks to be the most photoactive heterojunction due to its suitable electronic structure for the spatial separation of the photoinduced e⁻ and h⁺ carriers. Moreover, type-II heterojunction photocatalysts exhibit good e⁻ and h⁺ carriers separation efficiency, fast mass transfer and absorbance of light in the visible region with a band gap values under 2.8 eV [52]. In this sense, Prabhu et al. [53] synthesized djembe like ZnO microstructures by surfactant-assisted hydrothermal method,


(a)   (b)   (c)
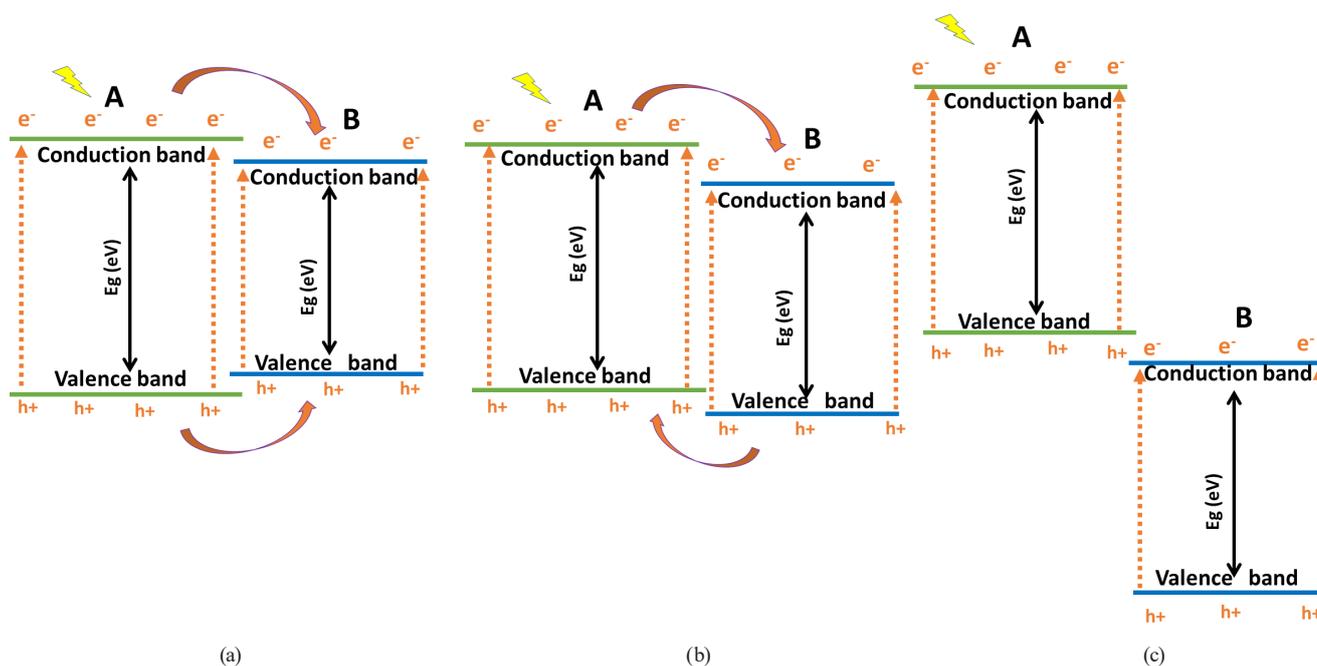
Fig. 4 The three conventional heterojunction types, (a) type-I, (b) type-II and (c) type-III. Adapted from [49].

and its composite with graphitic carbon nitride (g-C_3N_4) was prepared by ethanolic reflux method for the first time. The nanostructures were studied in the photodegradation of methlyne blue (MB) and rhodamine B (RhB). According to optical studies, the V_B potential and C_B potential were calculated as 2.83 eV and –0.64 eV for ZnO and 1.62 eV and –1.15 eV for g-C_3N_4. Due to the distinct positions of the V_B and C_B potentials between ZnO and g-C_3N_4, a type-II heterojunction was formed. The authors also mentioned that the heterojunction formed between djembe like ZnO and g-C_3N_4 decreased the optical band gap energy due to the light absorption was shifted towards the visible region. The degradation efficiency of the ZnO/g-C_3N_4 composite for MB and RhB degradation was found to be ~95% and ~97%, respectively, compared to the pure ZnO and g-C_3N_4. The authors proposed a possible visible-light-driven photocatalytic mechanism at the interface of ZnO/g-C_3N_4 heterojunction (Fig. 5, [53]). Pure ZnO semiconductor cannot be excited due to its wide bandgap (3.17 eV); only the g-C_3N_4 is excited by visible light to generate e$^-$ and h$^+$ carriers. Since the C_B edge potential (–1.15 eV) of g-C_3N_4 is more negative than that of ZnO (–0.64 eV), the photoexcited electrons in the CB of g-C_3N_4 are transferred to the CB of ZnO and then to the surface of the photocatalyst, by enhancing their photocatalytic properties.

Additionally, Ramezanalizadeh et al. [54] prepared through a sol-gel hydrothermal approach a novel $CoTiO_3$/$CuBi_2O_4$ heterojunction semiconductor photocatalyst for the degradation of Direct Red 16 dye under LED visible light irradiation. According to the authors, compared to the pure $CoTiO_3$ and $CuBi_2O_4$, $CoTiO_3$/$CuBi_2O_4$ heterojunction showed the highest photodegradation efficiency. Based on the obtained results, the $CoTiO_3$/$CuBi_2O_4$
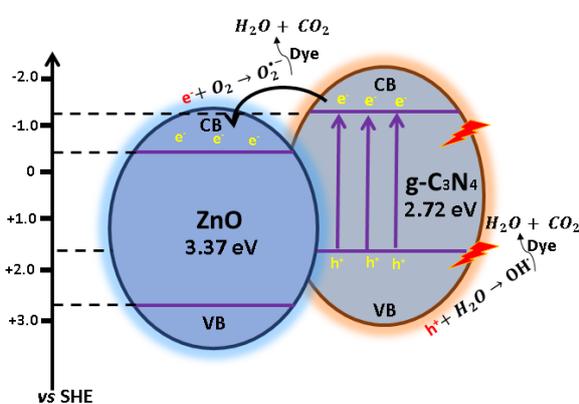

Fig. 5 Schematic representation of the photocatalytic mechanism over ZnO/g-C_3N_4 heterojunction. Adapted from [53].

heterojunction nanocomposites showed the highest removal efficiency (91%) in pH 4.3 solutions and at a loading of 5 g/L. This effect was attributed to the efficient separation of electron-hole pairs, compatible junction formation, visible light absorption ability, suitable band gap, and a large amount of light-harvesting. Moreover, according to the scavenger experiments, the pH played a major role during photocatalytic activity. Similarly, Chen et al. [55] prepared a photocatalyst of TiO_2 grown in situ on the surface of carbon nanotubes (CNT) for the photocatalytic degradation of Rhodamine B (Rh-B) under simulated sunlight synthesized by the sol-gel reflux method. The degradation efficiency of CNT-TiO_2 for Rh-B was 50% higher than pure TiO_2, and the addition of CNT increased the specific surface area, optical support, dispersibility, and uniformity of the synthetic material of the TiO_2 nanoparticles. The authors concluded that the n-n heterojunction structure was beneficial to accelerate the e$^-$ and h$^+$ carriers migration and improved the photocatalytic performance of the composite. In this study, the authors proposed that under the radiation of simulated sunlight, photoexcited electrons from TiO_2 C_B were transferred to the CNT structure, reducing the recombination process of the e$^-$ and h$^+$ carrieres.

4.3 The p–n heterojunctions

Although the heterojunction type-II seems to be the most effective way to avoid the recombination process due to the entrapment of photogenerated e$^-$ and h$^+$ carriers, it is not effective enough to avoid the fast recombination process. Hence, the p-n-type heterojunction model was proposed to explain the accelerated migration of photogenerated species through a generated electric field in the interface between p-type and n-type semiconductors by suppressing the recombination process [56]. A p–n junction is the interaction between two types of semiconductors photocatalytic materials (p-type and n-type) inside a single crystal of photocatalyst. The p-type semiconductor contains an excess of holes, and the n-type semiconductor contains an excess of electrons. Therefore, during irradiation, when electrons and holes are photo-created, the electrons of C_B from p-type semiconductor near of interface undergo diffusion towards C_B of n-type (positive field) and then reacted with O_2 adsorbed on the surface to produce reactive $O_2^{\cdot-}$. At the same time, the holes from the V_B of n-type semiconductor near interface tend to flow towards V_B of p-type (negative field) semiconductor, establishing the p-n junction (Fig. 6) [57].
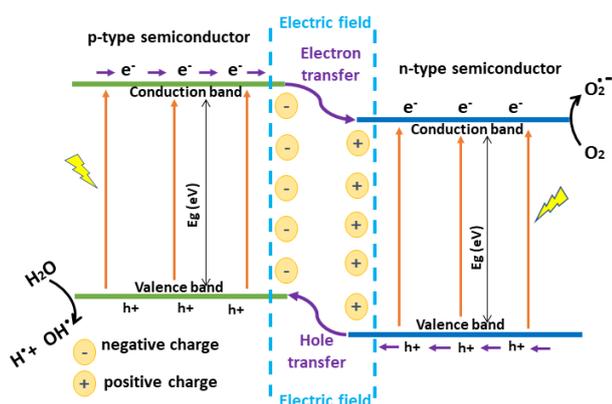
Fig. 6 Schematic diagram illustrating the formation and operation of the p–n junction (Adapted from [57])

The electron-hole transfer between n-type and p-type semiconductors is known as diffusion, and it will continue until the system's equilibrium state (e.g., Fermi level), reducing the recombination of the photogenerated charge carriers by the internal electric field at the p-n junction [58]. Moreover, the systems of p-n junctions are designed for operation under visible light, one of the goals of modern photocatalysis. Recently, Habibi-Yangjeh et al. [59] prepared $ZnO/ZnBi_2O_4$ (containing 5, 10, 20, and 30 wt% of $ZnBi_2O_4$) nanocomposites with p-n heterojunction fabricated by integrating ZnO with $ZnBi_2O_4$ nanoparticles via a calcination process for the photodegradation of RhB. The $ZnO/ZnBi_2O_4$ nanocomposites exhibited superior photocatalytic performance for the photodegradation of the organic dye under visible light compared with the pure ZnO and $ZnBi_2O_4$. The composite $ZnO/ZnBi_2O_4$ with 10 wt% achieved a photodegradation of 97% of the RhB dye after 240 min, whereas the pristine ZnO and $ZnBi_2O_4$ decomposed 28% and 39% of the RhB solution after 360 min, respectively. This enhancement can be ascribed to the efficient charge carrier separation through the heterojunction structure, which inhibits the recombination of photoinduced charges. The authors mentioned that an inner electrostatic field directed from ZnO to $ZnBi_2O_4$ was produced; moreover, in the presence of visible-light illumination, only $ZnBi_2O_4$ is excited, and the e^- and h^+ carriers are produced because of its narrow band gap. After the p-n heterojunction formation, the C_B level of $ZnBi_2O_4$ is more negative than that of ZnO. Hence, the excited electrons can inject into the C_B of ZnO, promoted by the inner electrostatic field, while holes remain in the VB of $ZnBi_2O_4$. Therefore, the photogenerated charge carriers can be separated effectively by the formed inner field of p-n heterojunction reducing the recombination of the e^- and h^+ carriers in the photocatalyst. In another work,

Sang et al. [60] reported the synthesis of heterostructured Bi_2O_3/Bi_2S_3 nanoflowers (1 to 2 μm of diameter) fabricated by a one-step hydrothermal method to remove of RhB and Cr(VI). The results of photocatalysis showed that removal efficiencies of RhB (99.7%) and Cr(VI) (91.8%) over Bi_2O_3/Bi_2S_3 heterojunction were higher than those of pure Bi_2O_3 and Bi_2S_3 (< 50% of removal) under visible light irradiation after 90 min of reaction. The improved photocatalytic performance of the Bi_2O_3/Bi_2S_3 heterojunctions was associated with the combination between components and their specific surface areas (46.3 m^2g^{-1}, 10.1 m^2g^{-1} and 12.6 m^2g^{-1}, respectively). Moreover, according to the radical trapping experiments, the photogenerated h^+ were the major oxidative species for removing RhB, while the photogenerated e^- were responsible for the photoreduction of Cr(VI). Authors argued that the excited e^- on the C_B of p-type Bi_2S_3 moves to n-type Bi_2O_3, while the photogenerated h^+ still stays in the V_B of p-type Bi_2S_3. In the Bi_2O_3/Bi_2S_3 photocatalytic system, the e^- and h^+ carriers are involved in the redox reaction. Therefore, for the system of Cr(VI) solution, the e^- provided by the C_B of n-type Bi_2O_3 is being effectively consumed by Cr(VI), which is a strong oxidant. On the other hand, the h^+ stayed on the V_B of Bi_2S_3 would oxidize the RhB molecules directly (Fig. 7); hence the h^+ is the predominant radicals, which oxide RhB to simpler molecules.

For its part, Lu et al. [61] prepared a series of $BiOI/KTaO_3$ p–n heterojunctions via a facile in situ chemical bath strategy for the degradation of Rhodamine B (RhB) under visible light irradiation. As a result, the $BiOI/KTaO_3$ composites showed higher photocatalytic efficiency compared to the individual catalysts. In particular, 54 wt% $BiOI/KTaO_3$
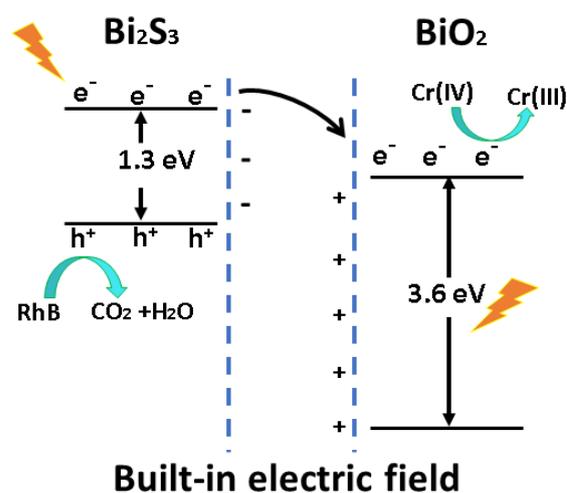

Fig. 7 Proposed mechanism for separation and transfer process of photogenerated carriers in the Bi_2O_3/Bi_2S_3. Adapted from [60].

degraded 98.6% RhB within 30 minutes withouth affecting its removal properties up to 3 cycles (91.1%), while only 68.1% RhB was degraded over pure BiOI. According to the authors, the improved photocatalytic performance was attributed to the successful construction of the p–n junction between BiOI and $KTaO_3$, facilitating the separation and migration of photo-induced charge carriers.

4.4 Direct Z-scheme

Yu et al. [62] proposed the concept of the direct Z-scheme mechanism to explain the process of the photocatalytic formaldehyde degradation in the TiO_2/g-C_3N_4 presence. The assembly of a direct Z-scheme photocatalyst (Fig. 8) looks like that of a type-II heterojunction (Fig. 4 (b)), but their e^- and h^+ charge carriers transport processes are somewhat different [63]. Furthermore, the direct Z-scheme system does not need a redox medium, and the photocarriers directly transfer across the interface of both semiconductors without a charge carrier intermediary. Therefore, the transmission distance is reduced, and the photocatalytic efficiency is enhanced. Under light irradiation, the photogenerated electrons in semiconductor A, with a lower reduction ability, recombine with the photogenerated holes in semiconductor B with a lower oxidation ability [64]. Thus, the photogenerated electrons in semiconductor B with high reduction ability and the photogenerated holes in semiconductor A with a high oxidation ability are kept in their particular sites to get the spatial separation of charge carriers to improve the redox capacity of the photocatalytic structure. In this manner, the charge-carrier migration is more promising than in type-II junction because the migration of electrons from the C_B of semiconductor A to the hole-rich V_B of semiconductor B is thermodynamically possible by the electrostatic attraction between the e^- and h^+. Direct Z-scheme offers advantages as fast e^- and h^+

carriers separation efficiency, good redox ability, corrosion resistance, and low fabrication cost [49, 65].

In this sense, Zhao et al. [66] prepared a Z-scheme heterogeneous g-C_3N_4/FeOCl photocatalysts using the calcination method. The composite with a morphology of a ribbon-like sheet was used to eliminate RhB from water. Compared with the pure FeOCl material (60% of RhB removal), the Z-scheme g-C_3N_4/FeOCl composites revealed a higher photocatalytic activity (90% of RhB removal) under visible light irradiationafter 60 minutes of reaction. The authors argued that the enhanced catalytic activity of the g-C_3N_4/FeOCl material was attributed to the formation of a Z-scheme between g-C_3N_4 and FeOCl (Fig. 9). Authors explained that when g-C_3N_4/FeOCl is irradiated with visible ligth, the electrons from the V_B of the g-C_3N_4 and FeOCl were transferred to their respective C_B. After that, the electrons were transferred from the C_B of FeOCl to the V_B of the g-C_3N_4 and combined with h^+. Then, these electrons transformed the H_2O_2 into the OH·. In this process, the H_2O_2 served as the electron acceptor which further successfully limited the recombination of holes and electrons. On the other hand, on the surface of the FeOCl material, the Fe^{3+} was transformed into Fe^{2+} with the presence of H_2O_2 and the irradiation of visible light; hence, the Fe^{2+} was easily reacted with H_2O_2 to generated the OH· for removing the pollutant. Due to the C_B of the g-C_3N_4 was more negative than $E^0(O_2/O_2^{\cdot-})$ and the V_B of the FeOCl was more positive than $E^0(OH·/OH^-)$, the


Fig. 9 The PF-like degradation mechanism of g-C_3N_4/FeOCl composite under the visible light irradiation. Adapted from [66].

Fig. 8 Electron-hole separation on a direct Z-scheme photocatalysts

electron which gathered on the C_B of the g-C_3N_4 would also reduce O_2 to form the $O_2^{•-}$ and the h^+ on the V_B of the FeOCl could oxide the OH^- into the $OH^•$ at the same time.

In other study, An et al. [67] prepared a core-shell Ag_2CO_3@g-C_3N_4 photocatalyst by two-dimensional coating nanosheet g-C_3N_4 on the surface of Ag_2CO_3 for the photodegradation of methyl orange (MO). According to the authors, the Ag_2CO_3@g-C_3N_4 (5 wt.%) composite exhibited the best degradation efficiency, up to 96.7% and 87.3% after five cycles. However, the photodegradation performance was in a g-C_3N_4 dose-dependent response (from 1 wt.% to 10 wt.%). The authors mentioned that the photocatalytic performance was due to the faster-photogenerated carrier migration efficiency derived from core-shell structure and chemical bond hybridization effect arising from Ag_2CO_3 and g-C_3N_4. Moreover, the excellent performance of photocatalyst was due to the Z-scheme structure formed by the Ag_2CO_3@g-C_3N_4 photocatalyst, which effectively avoids the accumulation of photoinduced electrons in the Ag_2CO_3 and inhibits Ag^+ photoreduction, which significantly improves the stability of Ag_2CO_3. Recently, Zhang et al. [68] reported a Z-scheme-based BiOI/CdS heterojunction with efficient photocatalytic degradation of RhB (20 mg/L) under visible light. The in-situ stirring and calcining method synthesized the Z-scheme-based BiOI/CdS heterojunction. Three BiOI/CdS composites were prepared (the mass ratio of BiOI to CdS was 60 wt.%, 80 wt.%, and 100 wt.%, respectively referred to as 0.6-BiOI/CdS, 0.8-BiOI/CdS, and 1.0-BiOI/CdS). The removal efficiency of RhB was BiOI < CdS < 1.0-BiOI/CdS < 0.6-BiOI/CdS < 0.8-BiOI/CdS. Moreover, after 4 cycles, the degradation of the 4th experiment reached 98% of the first, indicating the 0.8-BiOI/CdS composites exhibited excellent stability. According to the authors, the free radical capture experiments showed that $^•O$ was the main active substance in the degradation process.

4.5 The g-C_3N_4-based photocatalysts

The g-C_3N_4 is a characteristic material belonging to the second group of designed photocatalysts with a band gap of 2.7 eV, which means that operates under visible light. g-C_3N_4 shows a two-dimensional (2D) planar π conjugation structure, which could improve the electron transfer mechanism due to its prominent electronic activity [69]. In addition, due to its high nitrogen content, g-C_3N_4 may provide more active reaction sites than other N carbon materials by contributing to the photocatalytic reaction [70].

However, its fast recombination of the e^- and h^+ carriers reduces its photoactivity efficiency as only photocatalyst. Therefore, it is recommended that g-C_3N_4 be coupled to another semiconductor material to improve its photocatalytic activity by creating an interesting electronic structure as a whole. For example, Wei et al. [71], through the solvothermal method, synthesized the ternary heterojunction g-C_3N_4/Ag/ZnO with a 3D flower-like structure and 1.5 μm of diameter for the photodegradation of MO. The ternary heterojunction g-C_3N_4/Ag/ZnO photocatalytic activity was better compared to the pure g-C_3N_4, g-C_3N_4/ZnO composite, and g-C_3N_4/Ag composites. According to the authors, the plasma effect of Ag nanoparticles can be used to expand the response range of the photocatalyst to visible light. Meanwhile, Ag particles on the heterogeneous interface of g-C_3N_4 and ZnO play the role of conducting electrons, which are beneficial to separating of photogenerated electrons and holes. Zhao et al. [72] prepared a photocatalyst of Ag/$WO_{2.9}$/g-C_3N_4, demonstrating better adsorption capacity promotion than traditional WO_3. The composite was prepared by calcination and compared with the Ag/$WO_{2.9}$ and g-C_3N_4, the Ag/$WO_{2.9}$/g-C_3N_4 showed a graphite-like carbon nitride as a substrate, and nano-sheets $WO_{2.9}$ attached to silver nanoparticles are stacked on g-C_3N_4. This unique structure generated a large specific surface area, coupled with the oxygen deficiency inherent in $WO_{2.9}$, which favored the adsorption of dye molecules. Moreover, the photocatalytic tests (under visible light irradiation ($\lambda > 420$ nm)) on Ag/$WO_{2.9}$, g-C_3N_4, and Ag/$WO_{2.9}$/g-C_3N_4 showed that Ag/$WO_{2.9}$/g-C_3N_4 has the best adsorption activity and photocatalytic degradation ability under visible light conditions. The authors also mentioned that the formed photocatalyst constitutes a Z-scheme, which effectively separates the C_B region and the V_B region and performs efficient regional reaction. Likewise, Xue et al. [73] prepared a hetero-structured photocatalyst consisting of two-dimensional g-C_3N_4 nanosheets and commercial MoO_3 microparticles through a simple mixing and annealing process for the photodegradation of RhB. According to the authors, the MoO_3/g-C_3N_4 composite showed a significant improvement compared with individual MoO_3 or g-C_3N_4 and their physical mixture. Moreover, with the results of electron spin resonance, the authors concluded that a direct Z-scheme charge transfer between MoO_3 and g-C_3N_4 not only causes an accumulation of electrons in g-C_3N_4 and holes in MoO_3, but also boosts the formation of superoxide radicals and hydroxyl radicals. The total dye was photodegraded in 15 minutes

using 25 mg of catalyst dispersed into 50 mL of RhB solution (10 mg L^{-1}). In this context, several heterojunctions materias have been used for MO [66, 71, 72, 74–79], RhB [53, 59, 60, 61, 67, 72, 73, 78, 80–95], MB [53, 72, 75, 77, 94, 96–105] and other pulliting dyes [54, 75,100, 103, 106–118] removal, as shown in Table 2.

4.6 Immobilized photocatalysts

The typical suspended photocatalytic systems of powders show good mass transfer coefficients and the advantage of a greater surface area against the immobilized system. However, their disadvantage relies on the recovery of the powders after the photocatalytic reaction, increasing the process costs, which is a drawback [119]. In addition, the loss in the photoactivity of the recycled powders is another challenge related to the separation techniques. The immobilized systems take better advantage of the irradiated light and do not require a post-treatment for recovery the photocatalyst. The features of the semiconductor-active species and its interaction with the employed support are key factors to achieve a good photoactivity. Unfortunately, the immobilized system's configuration is only effective in arranging with a high surface-to-volume ratio, e.g., in microchannel reactors [120]. For example, Bahrudin et al. [121] studied the decolorization of methyl orange (MO) using immobilized TiO$_2$/chitosan-montmorillonite (TiO$_2$/CS-MT), a combination of TiO$_2$ as the top layer and CS-MT as the sub-layer on a glass plate. The authors mentioned that the immobilized CS-MT film showed better performance over the CS film since the former adhered stronger and swelled less than the latter, which showed its favorability in the aqueous medium. Moreover, the bilayer photocatalyst could remove the MO from the solution 3 times faster than the single TiO$_2$ within 90 min of irradiation under a UV–Vis lamp due to the strong adsorption of dye by the CS-MT sub-layer.

Ounas et al. [122] presented a simple and effective approach to prepare a polymethyl methacrylate–TiO$_2$ (TiO$_2$/PMMA) film photocatalyst, by a cheap and low-cost technique. The characterization of the film by XRD, FTIR, and Transmittance spectroscopy confirmed that the anatase TiO$_2$ has been deposited on the surface of the polymer. The film prepared was subsequently used in photodegradation of MB under artificial UV irradiation and showed a good prospect for the immobilization of TiO$_2$ intended for the photodegradation of pollutants generally present in waters. However, the authors mentioned that the method described can still be improved to

become easier and faster in a near future. Furthermore, de Araujo Scharnberg et al. [123] evaluated the photocatalytic properties of TiO$_2$ under porous ceramics support for the degradation of RhB. For this, the anatase TiO$_2$ calcined at 400 °C was prepared by the sol-gel method and supported in a porous ceramic substrate by a dip-coating process. The heterogeneous photocatalysis showed excellent results, with the degradation of up to 83% of RhB. The Authors also mentioned that after the usage, a major part of the catalyst stayed at ceramics, making possible to recover it, or to use the catalyst in a continuous flow reactor. Additionally, Inderyas et al. [124] reported that ZnO nanoparticles were immobilized on polyurethane foam (PUF) and employed for the degradation of Acid black 1 dye. In this study, the process variables like dye concentration, pH, the concentration of H$_2$O$_2$, irradiation time were optimized for maximum dye degradation. The ZnO/PUF showed high efficiency for the degradation of AB1 dye, and up to 86% and 65% dye degradation was achieved under UV and solar light irradiation at neutral pH, 4% H$_2$O$_2$, 240 min/sunlight, and 75 min/UV irradiation time using 40 mg L^{-1} dye initial concentration. Moreover, the reductions in BOD, COD, and TOC values confirmed that the ZnO/PUF was efficient. Das and Mahalingam [125] prepared a physical mixture of rGO and g-C$_3$N$_4$ along with TiO$_2$ (ratio of 1:1:1). The nanocomposites were immobilized in a polystyrene film using the facile solvent casting method for the degradation of remazol turquoise blue dye. The results using the immobilized catalyst mixture film gave 92.25% of TOC reduction, 94% of decolorization in 140 min, and a 72% of degradation in the fourth time of reuse.

In this sense, several supported photocatalysts have been prepared for MO [121, 126–130], RhB [123, 131–133], MB [122, 134–144], and other pulliting dyes [124, 125, 145–159] removal, as shown in Table 3.

5 Influence of operational parameters on the photocatalytic degradation

According to the evidence, the photocatalysts synthesized by different methods are attractive materials with high photocatalytic properties for diverse dye degradation from water. However, their effects are in a shape-, size- and dose-dependent response. In general, these materials are low-cost, efficient, reusable, and environmentally friendly for wastewater treatment. Additionally, the efficiency of these materials mainly depends on the experimental conditions, as discussed in Subsections 5.1–5.6.

Table 2 Photocatalytic studies about dyes degradation using heterojunctions

No.	Photocatalyst	Synthesis method	Morphology	Size (nm)	Band gap (eV)	Light	Dye	Time (min)	Degradation (%)	Ref.
1	$SrTiO_3$-BiOI	Microwave-assisted solvothermal	Fibers	-	1.9–2.3	Vis	Methyl orange	180	94.6	[74]
2	g-C_3N_4/Ag/ZnO	Solvothermal	Flower	150	-	Vis	Methyl orange	180	58.1	[71]
3	Ag_2CO_3@g-C_3N_4	Coating two-dimensional	Ribbon-sheet	-	-	Vis	Methyl orange	54	96.7	[66]
4	$CoFe_2O_4$/MoS_2	Electrospinning and hydrothermal	Nano rod/flower like	-	1.26–1.01	Vis	Methyl orange	60	67.5	[75]
5	BiOCl/$Ag_8Si_2O_7$	Deposition–precipitation	Spherical	-	1.87	Vis	Methyl orange	40	98.1	[76]
6	BiOBr/$Ag_6Si_2O_7$	Hydrothermal	Flake/irregular	-	2.41–2.54	Vis	Methyl orange	20	96	[77]
7	$BiFeO_3$/$CuWO_4$	Impregnation	Wafer-like/grain-like	-	2.2	Vis	Methyl orange	120	85	[78]
8	g-C_3N_4/Ag_3PO_4	Calcination and precipitating	Sheet/irregular spherical	-	-	vis	Methyl orange	30	95	[79]
9	$WO_{2.9}$/g-C_3N_4	Calcination	Nanosheet stack	150–50	-	Vis	Methyl orange	270	≈95	[72]
10	$WO_{2.9}$/g-C_3N_4	Calcination	Nanosheet stack	150–50	-	Vis	Rhodamine B	270	≈91	[72]
11	g-C_3N_4/Ag_3PO_4	Calcination and precipitating	Sheet/irregular spherical	-	-	Vis	Rhodamine B	15	96	[79]
12	MoO_3/g-C_3N_4	Mixing and annealing	Porous and lamellar structure	-	2.81	Vis	Rhodamine B	15	100	[73]
13	ZnS/bulk g-C_3N_4	In-situ hydrothermal	Irregular	-	-	Vis	Rhodamine B	90	99	[80]
14	Bi_2MoO_6/WO_3/Ag_3PO_4	One-step hydrothermal	Sheet/rod/sphere	-	2.33	Vis	Rhodamine B	120	97.31	[81]
15	$NaTaO_3$/g-C_3N_4/G	In-situ calcination and photochemical reduction	Sheet/nanocubes	-	-	Vis	Rhodamine B	70	99	[82]
16	Fe_2O_3/C-g-C_3N_4	One-step carbonizing	-	-	-	Vis	Rhodamine B	80	95	[83]
17	TiO_2 modified rod-like g-C_3N_4	One-pot hydrothermal	Rod/spherical	25–35	2.45	Vis	Rhodamine B	240	98.6	[84]
18	Bi_2O_3/Bi_2S	One-step hydrothermal	Nanoflower	1000–2000	3.38–1.44	Vis	Rhodamine B	90	99.72	[60]
19	BiOI/$KTaO_3$	Hydrothermal and chemical bath	Nanosheets/cubes	-	-	Vis	Rhodamine B	30	98.6	[61]
20	$Sm_2Ti_2O_7$	Biopolymer - mediated	Spherical	12	2.6	Vis	Rhodamine B	80	94	[85]
21	$Bi_xSb_{2-x}S_3$	Hydrothermal	Rod	37	2.4–2.9	Vis	Rhodamine B	30	97	[86]
22	ZnO/$ZnBi_2O_4$	Refluxing route and calcination	Rice-like/spherical	-	-	Vis	Rhodamine B	240	97	[59]
23	α-β Bi_2O_3	Solvothermal	Spherical and rods/nano flakes/flower like	24–126	2.35–3.19	Vis	Rhodamine B	120	99.6	[87]
24	Ag_3PO_4/$BiNbO_4$	Co-precipitation	Spherical/irregular	350/100	3.24	Vis	Rhodamine B	30	98.8	[88]
25	NiO/BiOI	Solvothermal	Foam-like/microspheres	-	-	Vis	Rhodamine B	60	90	[89]
26	TiO_2/AgBr/ polyaniline	Ultrasound	Irregular spheres	-	1.85	Vis	Rhodamine B	140	98.6	[90]
27	$Zn_3(VO_4)_2$/$FeVO_4$	Hydrothermal	Rod/flower	-	2.01	Vis	Rhodamine B	90	100	[91]
28	BiOCl/Bi–Bi_2O_3	Hydrothermal	Square nanosheets	20–20	3.15	Vis	Rhodamine B	60	> 90	[92]
29	MoO_3/Bi_2O_4	Hydrothermal	Grain/nanorods	-	-	Vis	Rhodamine B	40	99.6	[93]
30	g-C_3N_4/FeOCl	Calcination	Nanosheets attached to Ag_2CO_3 rod surface	-	-	Vis	Rhodamine B	60	90	[67]
31	$BiFeO_3$/$CuWO_4$	Impregnation	Wafer-like/grain-like	-	2.2	Vis	Rhodamine B	120	87	[78]

No.	Photocatalyst	Synthesis method	Morphology	Size (nm)	Band gap (eV)	Light	Dye	Time (min)	Degradation (%)	Ref.
32	$ZnO/g\text{-}C_3N$	Hydrothermal	Djembe like	-	3.07	Vis	Rhodamine B	50	95	[53]
33	$AgI/BiVO_4$	Hydrothermal	Irregularly shaped blocks	-	2.27–2.34	Vis	Rhodamine B	80	89	[94]
34	$Ag_3PO_4/NaTaO_3$	Hydrothermal				Vis	Rhodamine B	25	99	[95]
35	$AgI/BiVO_4$	Hydrothermal	Irregularly shaped blocks	-	2.27–2.34	Vis	Methylene blue	80	99	[94]
36	$ZnO/g\text{-}C_3N$	Hydrothermal	Djembe like	-	3.07	Vis	Methylene blue	50	97	[53]
37	N doped TiO_2 (N/TiO_2)	Sol–gel approach	Spherical	14–18	2.91	Vis	Methylene blue	100	97	[96]
38	$Fe_3O_4/FeWO_4$	Hydrothermal	Nanowires/nanoparticles	200–500	2.5	Vis	Methylene blue	60	97.1	[97]
39	TiO_2/NiO	Hydrothermal	Nanosheet/nanorod	20~40	-	Vis	Methylene blue	100	100	[98]
40	$CaWO_4/\alpha\text{-}Ag_2WO_4$	One-step hydrothermal	Irregular	-	2.79–3.57	Vis	Methylene blue	105	85	[99]
41	$BiOBr/Ag_6Si_2O_7$	Hydrothermal	Flakes	-	2.57–2.54	Vis	Methylene blue	15	98	[77]
42	$WO_{2.9}/g\text{-}C_3N_4$	Calcination	Sheet stack	150–50	-	Vis	Methylene blue	270	≈ 93.5	[72]
43	$CoFe_2O_4/MoS_2$	Electrospinning and hydrothermal	Nano rod/flower like	-	1.26–1.01	Vis	Methylene blue	60	48.9	[75]
44	$g\text{-}C_3N_4/MnV_2O_6$	Hydrothermal	Layer/rod	-	-	Vis	Methylene blue	210	95	[100]
45	$Bi_2WO_6/r\text{-}GO/Bi_{25}FeO_{40}$	Hydrothermal	Nanoshees/flake/nanorod	-	-	Vis	Methylene blue	30	98.1	[101]
46	$g\text{-}C_3N_4@Zn_{0.5}Cd_{0.5}S$	Co-precipitation hydrothermal	Layer	40–80	2.51–2.8	Vis	Methylene blue	240	99.9	[102]
47	$Ag/Mn_3O_4/graphene$	Sol–gel and hydrothermal	Spherical	-	-	Vis	Methylene blue	120	97.3	[103]
48	$Ag/AgBr/LaAlO_3$	Deposition	Spherical/flake	-	2.65	Vis	Methylene blue	60	89	[104]
49	$Cu_2O@HNbWO_6$	Solution redox	Spherical/Layer	-	-	Vis	Methylene blue	120	90	[105]
50	$Ag/Mn_3O_4/graphene$	Sol–gel and hydrothermal	Spherical/irregular/sheet	-	-	Vis	Congo red	120	98.8	[103]
51	$CoFe_2O_4/MoS_2$	Electrospinning and hydrothermal	Nano rod/flower like	-	1.26–1.01	Vis	Congo red	60	94.9	[75]
52	$PSCN/Ag@AgI/WO_3$	One-pot precipitation	Irregular/sheet	-	-	Vis	Malachite green	60	90	[106]
53	$CdS/CdWO_4$	Ultrasound and precipitation	Nanorod/short rod	1–35	2.34–2.25, 2.32–2.33	Vis	Malachite green	100	97	[107]

No.	Photocatalyst	Synthesis method	Morphology	Size (nm)	Band gap (eV)	Light	Dye	Time (min)	Degradation (%)	Ref.
54	2D/1D g-C$_3$N$_4$/CaTiO$_3$	Solvothermal and calcination	Sheet/square tubular	-	-	Vis	Malachite green	90	95.02	[108]
55	2D/1D g-C$_3$N$_4$/CaTiO$_3$	Solvothermal and calcination	Sheet/square tubular	-	-	Vis	Crystal violet	180	99.76	[108]
56	ZnMoO$_4$/BiFeWO$_6$/RGO	Dispersion and ultrasound	Spherical, diamond, and hexagonal-like particles/sheet	-	-	Vis	Acid blue 25	180	98	[109]
57	g-C$_3$N$_4$/MnV$_2$O$_6$	Hydrothermal	Layer/rod	-	-	Vis	Indigo Carmine	210	94	[100]
58	g-C$_3$N$_4$-melamine-urea	Thermal polycondensation	Layers	-	2.82–2.86	Vis	Reactive orange 16	100	95	[110]
59	Sr/Ag-TiO$_2$@g-C$_3$N	Sol-gel and hydrothermal	Flake	-	-	Vis	Reactive black-42	40	95.6	[111]
60	Ni foam@ZnO/MoS$_2$	Two-step electrodeposition	Sheet	53.6–67.6	-	Vis	Acid Red 1	40	83	[112]
61	CoTiO$_3$/CuBi$_2$O$_4$	Sol-gel/hydrothermal	Flower-like	-	1.9	Vis	Direct red 16	90	91	[54]
62	YMnO$_3$/CeO$_2$	Sonochemistry method	Ball	-	2.82–2.51	Vis	Methyl red	240	99	[113]
63	Ag$_3$VO$_4$/Cu-MOF/rGO	Solvothermal	Particles/nanosheet	-	-	Vis	Acid blue 92	120	78	[114]
64	p-Ag$_3$PO$_4$/n-BiFeO$_3$	Precipitation	Sphere/cuboid	-	2.18	Vis	Acid orange 7	120	91	[115]
65	ZnO NP's/polypyrrole	Precipitation and chemical oxidation	Spherical	-	-	Vis	Orange II	30	100	[116]
66	Ag@AgBr/Bi$_2$MoO$_6$	Chemical deposition-light reduction	Flake/flower	-	2.78	Vis	Reactive blue 19	120	98.7	[117]
67	MoS$_2$/BiPO	Hydrothermal	Rods	-	-	Vis	Brilliant green	70	80	[118]

Table 3 Photocatalytic studies about dyes degradation using immobilized photocatalysts

No.	Photocatalyst	Substrate	Synthesis method	Morphology	Light	Dye	Time (min)	Degradation (%)	Ref.
1	TiO_2	Polyether sulfone matrix	Phase inversion technique	Tear and finger	UV	Methyl orange	540	80	[126]
2	$BaWO_4$	MOF-199-NH$_2$	Hydrothermal	Octahedral	UV	Methyl orange	80	98	[127]
3	γ-Fe_2O_3	Ni substrate	Autoclave	Rods and spheres	UV	Methyl orange	540	98	[128]
4	S, N-codoped TiO_2	Glass beads	Sol–gel and Dip coating	Irregular	Vis	Methyl orange	180	90	[129]
5	TiO_2	Chitosan-montmorillonite	Dip-coating	Flakes	Vis	Methyl orange	90	84	[121]
6	TiO_2/MgO	Chitosan-Hydrogel	Dropping	Granular	UV	Methyl orange	90	82.4	[130]
7	Au-TiO_2	Cellulose membranes	Tape and the suction filtration	Spherical	Vis	Rhodamine B	300	95	[131]
8	BiOCl	Bi plate	Ionic nucleation	Microspheres	Vis	Rhodamine B	210	98	[132]
9	TiO_2	Diatomite	Sol-gel	Disks	UV	Rhodamine B	120	92.6	[133]
10	TiO_2	Porous ceramic	Dip-coating	Porous net	UV	Rhodamine B	300	83	[123]
11	TiO_2-P25	Borosilicate glass spheres	Pip-coating	Microspheres	Solar irradiation	Methylene blue	90	96	[134]
12	TiO_2	ZSM-5 zeolite with nickel nanoparticles	Sol-gel	Semispherical	UV	Methylene blue	120	99.8	[135]
13	Rutile TiO_2	Basil seed	Hydrothermal and Coating process	Rods	UV	Methylene blue	120	98.9	[136]
14	Sintered commercial TiO_2	Basil seed	Coating process	Spheres	UV	Methylene blue	120	97.9	[136]
15	TiO_2	Poly methyl methacrylate	-	-	UV	Methylene blue	200	70	[122]
16	Chitosan-Polydimethylsiloxane-SiO_2-TiO_2	Pumice stones	Modified hydrothermal	Amorphous	Simulated sunlight	Methylene blue	1,800	64	[137]
17	Erbium-doped TiO_2	Macro-porous silica films	Sol-gel and ultrasonic bath	Irregular	Vis	Methylene blue	60	100	[138]
18	Carbon-doped TiO_2	Polyamide fibers	Electrospinning	Granular	Vis	Methylene blue	300	82.6	[139]
19	TiO_2/PEG (polyethylene glycol)	Double-sided adhesive tape	Brush technique	Porous	Vis	Methylene blue	75	100	[140]
20	Co-tetracarboxyl-phthalocyanine	Chitosan-Fe_3O_4	Immersion	Spherical	Vis	Methylene blue	300	90	[141]
21	TiO_2	Steel mesh	Electrospraying and hot-pressing	Spherical	UV	Methylene blue	40	100	[142]
22	TiO_2 and ZnO	Poly(vinylidene difluoride)-cotrifluoroethylene	Solvent casting	Rectangular	UV	Methylene blue	300	85	[143]
23	TiO_2	Polypropylene copolymer	Electrostatic-heating coating	Granular	Sunlight	Methylene blue	5,760	99.30	[144]
24	TiO_2	Grape marc–based activated carbon	Chemical activation and impregnation	Flakes	UV	Reactive black 5	60	98.9	[145]
25	TiO_2-P25	Polyethylene terephthalate	Wash coating of a TiO_2 suspension	Grooves and sheets	Simulated sunlight	Reactive Black 5	240	78	[146]
26	Fe-Ce-N tri-doped TiO_2	Glass bed	Sol-gel	Spherical	Vis	Direct Blue 15	60	99	[147]

No.	Photocatalyst	Substrate	Synthesis method	Morphology	Light	Dye	Time (min)	Degradation (%)	Ref.
27	Fe_2O_3/TiO_2	Carbon fiber cloth	Spraying process	Granular	Vis	Basic blue 41	240	97.5	[148]
28	ZnO and polypyrrole	Silica ring	Polymerization	Smooth flakes	Vis	Violet 7	360	64	[149]
29	Mixture of TiO_2, rGO and g-C_3N_4	Polystyrene	Facile solvent casting	-	UV	Remazol turquoise blue	140	94	[125]
30	Au-Pd	Hydrocalcites containing Ni(II) and Fe(III)	Co-precipitation and Sol-immobilisation	Lamellar	UV	Orange II	60	95	[150]
31	ZnO/Zn	Photoanode	Heat attachment	Rods	UV	Reactive green 19	480	100	[151]
32	TiO_2	GO electrode	Electrochemical deposition	Spherical and layers	UV	Acid red 14	120	96.3	[152]
33	TiO_2	Indium tin oxide	Spin-coating process	Granular	UV	Basic blue 26	60	91.2	[153]
34	ZnO	Polyurethane	Hydrothermal	Symmetrical	UV	Acid black 1	75	86	[124]
35	TiO_2	Reticulated Al_2O_3 ceramics	Dipping method	Granular	UV	Reactive orange 16	75	99	[154]
36	TiO_2:ZnO	Spacer fabrics	Cold plasma discharge	-	UV	Reactive orange 16	60	81	[155]
37	TiO_2/chitosan	Glass support	Dip-coating	-	Vis	Reactive Red 4	60	100	[156]
38	TiO_2 double-sided adhesive tape (DSAT)	Glass plate	Brush technique	Porous and granular	UV	Reactive Red 4	30	55	[157]
39	TiO_2 (P-25)	Glass	Ultrasonic sedimentation	Particulate layers	UV	Acid orange 7	120	80	[158]
40	TiO_2-P25 Degussa	Glass fibre mat	Impregnation	Fibreglass mat	UV	Acid orange 7	40	90	[159]

5.1 The pH influence

The pH of the solution in photocatalytic reactions determines electrostatic properties such as the surface charge of the photocatalyst, formation of hydroxyl radicals, size of the aggregates that it forms, and the band edge position of metal oxides used as photocatalysts [160]. Furthermore, the pH can influence the adsorption–desorption characteristics of the catalyst surface [161]. The photocatalyst surface can be protonated and deprotonated under acidic and alkaline conditions, respectively (Eqs. (7) and (8)):

$$MOH + H^+ \rightarrow MOH_2^+ \tag{7}$$

$$MOH + OH^- \rightarrow MO^- + H_2O. \tag{8}$$

The operating pH affects the isoelectric point and the surface charge of the photocatalyst. The reaction occurs at a different pH values from the isoelectric point (point of zero charges, pzc) where the surface of the material is not charged; under this value, the material is positively charged, and above this value, the catalyst is negatively charged. At pH > pzc, the adsorption of positively charged contaminants is preferred, while at pH < pzc, the adsorption of negatively charged contaminants is favored [162]. Values close to neutrality have no significant effect on the operation. Although the pH primarily affects the adsorption of charged contaminants, it also has a role in the photocatalysis of those neutral molecules that tend to dissociate into charged species. Therefore, the pH affects the surface of the photocatalyst and the dissociation of the dye [163].

5.2 Process temperature

In most photodegradation reactions, these are carried out at STP and do not require cooling or heating of the reaction system due to the photonic activation. Preferably the reactions should occur between 20 °C and 80 °C, since at high temperature ($T \geq 80$ °C), the recombination process of charge carriers is favored. Furthermore, the exothermic adsorption of reactant is not favored and tends to become the rate-limiting step [162, 164]. The increasing temperature does not favor adsorption, which becomes the inhibitor of the reaction, while at low temperature, inefficient desorption of final products is presented, and an increment in the activation energy is required to carry out the reaction [165]. Therefore, there is no need to waste energy for heating water that possesses a high heat capacity.

5.3 Photocatalysts loading

When the catalyst loading is increased, there is an increase in the contact surface of the catalyst, and a variation of the average dye–photocatalyst ratio could generate losses in the surface area by aggregation (particle–particle interactions) due to excess of the solid concentration causing a decrease in the number of exposed active surface sites [160]. The decrease of degradation at higher catalyst loading may be due to the deactivation of activated molecules by collision with ground-state molecules [166]. Moreover, with the increment of photocatalyst loading, UV light penetration can be reduced due to saturation of the aqueous medium, affecting the photodegradation rates [163]. Therefore, an optimum amount of photocatalyst must be used to ensure total absorption of light photons and avoid unnecessary excess. A constant agitation with a magnetic stirrer at the reactor base and an air flux bubbled continuously inside the reactor to provide enough O_2 are recommended to keep powder particles fluidization.

5.4 Dye concentration

The dye degradation rate under photocatalytic processes depends on its initial concentration [167]. When the initial dye concentration is increased, many molecules are adsorbed on the catalyst surface, and this may promote an inhibiting effect on the reaction of the dye with photogenerated holes or hydroxyl radicals because of the lack of any direct contact between them [168]. Furthermore, when the concentration of dye is increased, the dye molecules adsorb light (UV-screening effect), and the photons hardly reach the photocatalyst surface. Thus, the photodegradation efficiency decreases. On the other hand, the Langmuir-Hinshelwood model describes the kinetics of photocatalytic reactions of aquatic organics pollutants [169]; this model is based on the next assumptions:

1. limited surface adsorption sites,
2. only single layer adsorption, and
3. no interactions between molecules after adsorption.

Langmuir-Hinshelwood model is expressed as:

$$r = -\left(dC/dT\right) = \left(k_r k_{ad} C\right)/\left(1 + k_{ad} C\right), \tag{9}$$

where C is the concentration of aquatic organic, k_{ad} is the adsorption equilibrium constant and k_r is the intrinsic rate constant, which takes into account parameters such as catalyst mass, efficient photon flow, O_2 layer, etc. [170]. When

the concentration of dye is so low (millimolar), the Eq. (9) can be simplified to an apparent first-order equation [171]:

$$\ln\left(C/C_o\right) = -k_r k_{ad} t = -k_{app} t . \tag{10}$$

The linear region can be obtained from the plot of $\ln(C/C_o)$ vs t, in which the slope gives the rate constant of photodegradation. The half-life time (degradation of dye to its 50%) is calculated as:

$$t_{1/2} = \left(\ln\left(2\right)\right)/k_{app} . \tag{11}$$

5.5 Light source and intensity
Relatively high light intensity is required to provide photocatalyst particle enough photons energy. Hence, it is essential to establish the range of radiation with which the solution must be irradiated. It has been shown that the reaction rate is proportional to the radiant flux Φ. However, above a certain value, the reaction rate becomes proportional to $\Phi^{1/2}$, indicating strong electron-hole recombination. In this context, Ollis et al. [172] studied the effect of light intensity on the kinetics of the photocatalytic reaction, and the following results were found:

1. At low light intensities (0–20 mW/cm^2), the rate would increase linearly with increasing light intensity (first-order) due to reactions involving e$^-$ and h$^+$ carriers formation is predominant.
2. At intermediate light intensities beyond a certain value (≈ 25 mW/cm^2), the rate would depend on the square root of the light intensity (half order) because the e$^-$ and h$^+$ carriers separation compete with recombination causing a lower effect on the reaction rate.
3. At high light intensities, the rate is independent of light intensity if the temperature is low.

Other important factor is the lamp-reactor geometry where the reaction takes place; the geometry and fabrication materials could favor the homogeneous dispersion of the light.

5.6 Disadvantages and perspectives in photocatalysis
Even though researchers have made tremendous progress in the photocatalysis field, some challenges remain about the operation of photocatalysts in industrial applications. For example, the light distribution inside the reactor and the configuration of the reactor are the main issues to be addressed. According to Ahmad et al. [173], the scaling-up of a photocatalytic reactor has been limited due to the reactor design have not been able to address the two most

important strictures; light distribution inside the reactor through absorbing and scattering liquid to the photocatalyst, and to provide high surface areas for photocatalysts coating per unit reactor volume. In addition, the costs of incident photon production must be considered in the process economy when talking about treating huge volumes of wastewater. Furthermore, the chemical restrictions play a crucial role in the performance of dye removal such as the interfacial charge transfer, improve the charge carriers separation, and the inhibition of charge carriers recombination process. Some challenges like mass transfer limitations, catalyst deactivation, generation of intermediate products and by-products, and the multi-complex optimization of the materials and the reactor configuration limit the real industrial applications. On the other hand, several trends for further development are currently under investigation. These trends include:

1. The development of economical methods for the preparation at large scale of nanomaterials with controlled morphology.
2. The development of the characterization techniques and instruments to elucidate and confirming the migration pathways of electron-hole pairs in heterojunction photocatalyst.
3. The hybridation with photocatalytic components in a single device.
4. The fine control of increasingly complex nanoarchitectures and (v) the use of novel non-oxidic materials.

According to the literature, there are some challenges to be achieved for scaling up applications of photocatalysts. However, their use for dye degradation is an active research area with potential applications as an alternative for wastewater treatment. Therefore, further research efforts should be dedicated to solving these challenges.

6 Concluding remarks
According to the evidence, the potential application of photocatalysis is an efficient alternative to remove dyes from water. Most recent works reported promising degradation results (> 90% of dye degradation) in shorter reaction times. Nevertheless, the search for photocatalysts with desired characteristics to induce the total oxidation of dye molecules under visible light irradiation in an economically accessible way is encouraging. From the transition of single component photocatalysts to the design and application of heterojunctions and immobilized photocatalytic systems, important problems were solved, such as

extending the life of the photogenerated species and the use of a lower photocatalytic powder amount per volume of wastewater. In addition, the design of immobilized photocatalysts also solved problems such as powder separation and recovery stages. However, it attracted new challenges (e.g., reduction of surface area). At present, the demand for environmental sustainability that humanity is facing has forced researchers to design photocatalytic systems that avoid the recombination process, with various life cycles and low cost energetic, easy to manufacture, and economically accessible at laboratory scale. An ideal photocatalyst should fulfill requirements such as visible-light activity, high solar energy conversion efficiency, proper band gap structure for redox reactions, high photostability for long-term applications, and scalability for commercialization. In fact, several researching groups agree that the design of active nanostructures under visible light is one of the main challenges for the development of these materials. Some current limitations may be resolved in the future, by coupling photocatalysis with other emerging technologies.

Acknowledgments

References

[1] Santos-Ebinuma, V. C., Roberto, I. C., Simas Teixeira, M. F., Pessoa, A. "Improving of red colorants production by a new Penicillium purpurogenum strain in submerged culture and the effect of different parameters in their stability", Biotechnology Progress, 29(3), pp. 778–785, 2013.
https://doi.org/10.1002/btpr.1720

[2] Bulut, M. O., Akar, E. "Ecological dyeing with some plant pulps on woolen yarn and cationized cotton fabric", Journal of Cleaner Production, 32, pp. 1–9, 2012.
https://doi.org/10.1016/j.jclepro.2012.03.010

[3] Rauf, M. A., Ashraf, S. S. "Survey of recent trends in biochemically assisted degradation of dyes", Chemical Engineering Journal, 209, pp. 520–530, 2012.
https://doi.org/10.1016/j.cej.2012.08.015

[4] Hassaan, M. A., El Nemr, A. "Health and Environmental Impacts of Dyes: Mini Review", American Journal of Environmental Science and Engineering, 1(3), pp. 64–67, 2017.
https://doi.org/10.11648/j.ajese.20170103.11

[5] Martini, J., Orge, C. A., Faria, J. L., Pereira, M. F. R. Soares, O. S. G. P. "Sulfamethoxazole degradation by combination of advanced oxidation processes", Journal of Environmental Chemical Engineering, 6(4), pp. 4054–4060, 2018.
https://doi.org/10.1016/j.jece.2018.05.047

[6] Chang, H. H., Cheng, T.-J., Huang, C.-P., Wang, G.-S. "Characterization of titanium dioxide nanoparticle removal in simulated drinking water treatment processes", Science of The Total Environment, 601–602(17), pp. 886–894, 2017.
https://doi.org/10.1016/j.scitotenv.2017.05.228

[7] Katheresan, V., Kansedo, J., Lau, S. Y. "Efficiency of various recent wastewater dye removal methods: A review", Journal of Environmental Chemical Engineering, 6(4), pp. 4676–4697, 2018.
https://doi.org/10.1016/j.jece.2018.06.060

[8] Barak, A., Goel, Y., Kumar, R., Shukla, S. K. "Removal of methyl orange over TiO_2/polyacrylamide hydrogel", Materials Today: Proceedings, 12, pp. 529–535, 2019.
https://doi.org/10.1016/j.matpr.2019.03.094

[9] Hameed, B. B., Ismail, Z. Z. "Decolorization, biodegradation and detoxification of reactive red azo dye using non-adapted immobilized mixed cells", Biochemical Engineering Journal, 137, pp. 71–77, 2018.
https://doi.org/10.1016/j.bej.2018.05.018

[10] Bilińska, L., Gmurek, M., Ledakowicz, S. "Textile wastewater treatment by AOPs for brine reuse", Process Safety and Environmental Protection, 109, pp. 420–428, 2017.
https://doi.org/10.1016/j.psep.2017.04.019

[11] Ben Mansour, H., Houas, I., Montassar, F., Ghedira, K., Barillier, D., Mosrati, R., Chekir-Ghedira, L. "Alteration of in vitro and acute in vivo toxicity of textile dyeing wastewater after chemical and biological remediation", Environmental Science and Pollution Research, 19(7), pp. 2634–2643, 2012.
https://doi.org/10.1007/s11356-012-0802-7

[12] Kant, R. "Textile dyeing and printing industry: An environmental hazard", Natural Science 4(1), pp. 22–26, 2012.
https://doi.org/10.4236/ns.2012.41004

[13] Fujishima A., Honda, K. "Electrochemical photolysis of water at a semiconductor electrode", Nature, 238(5358), pp. 37–38, 1972.
https://doi.org/10.1038/238037a0

[14] Dong, H., Zeng, G., Tang, L., Fan, C., Zhang, C., He, X., He, Y. "An overview on limitations of TiO_2-based particles for photocatalytic degradation of organic pollutants and the corresponding countermeasures", Water Research, 79, pp. 128–146, 2015.
https://doi.org/10.1016/j.watres.2015.04.038

[15] Byrne, C., Subramanian, G., Pillai, S. C. "Recent advances in photocatalysis for environmental applications", Journal of Environmental Chemical Engineering, 6(3), pp. 3531–3555, 2018.
https://doi.org/10.1016/j.jece.2017.07.080

[16] Di Mauro, A., Fragala, M. E., Privitera, V., Impellizzeri, G. "ZnO for application in photocatalysis: From thin films to nanostructures", Materials Science in Semiconductor Processing, 69, pp. 44–51, 2017.
https://doi.org/10.1016/j.mssp.2017.03.029

[17] Hisatomi, T., Kubota, J., Domen, K. "Recent advances in semiconductors for photocatalytic and photoelectrochemical water splitting", Chemical Society Reviews, 43(22), pp. 7520–7535, 2014.
https://doi.org/10.1039/C3CS60378D

[18] Molinari, R., Lavorato, C., Argurio, P. "Recent progress of photocatalytic membrane reactors in water treatment and in synthesis of organic compounds. A review", Catalysis Today, 281(1), pp. 144–164, 2017.
https://doi.org/10.1016/j.cattod.2016.06.047

[19] Ni, M., Leung, M. K. H., Leung, D. Y. C., Sumathy, K. "A review and recent developments in photocatalytic water-splitting using TiO_2 for hydrogen production", Renewable and Sustainable Energy Reviews, 11(3), pp. 401–425, 2007.
https://doi.org/10.1016/j.rser.2005.01.009

[20] AlKahtani, R. N. "The implications and applications of nanotechnology in dentistry: A review", The Saudi Dental Journal, 30(2), pp. 107–116, 2018.
https://doi.org/10.1016/j.sdentj.2018.01.002

[21] Ayodhya, D., Veerabhadram, G. "A review on recent advances in photodegradation of dyes using doped and heterojunction based semiconductor metal sulfide nanostructures for environmental protection", Materials Today Energy, 9, pp. 83–113, 2018.
https://doi.org/10.1016/j.mtener.2018.05.007

[22] Dahman, Y. "An Introduction to Nanotechnology*", In: Nanotechnology and Functional Materials for Engineers, Elsevier, Amsterdam, Netherlands, 2017, pp. 1–17.
https://doi.org/10.1016/B978-0-323-51256-5.00001-0

[23] Kusior, A., Banas, J., Trenczek-Zajac, A., Zubrzycka, P., Micek-Ilnicka, A., Radecka, M. "Structural properties of TiO_2 nanomaterials", Journal of Molecular Structure, 1157, pp. 327–336, 2018.
https://doi.org/10.1016/j.molstruc.2017.12.064

[24] Zanella, R. "Metodologías para la síntesis de nanopartículas: controlando forma y tamaño" (Methodologies for nanoparticle synthesis: shape and size control), Mundo Nano. Revista Interdisciplinaria en Nanociencia y Nanotecnología, 5(1), pp. 69–81, 2012. (in Spanish)
https://doi.org/10.22201/ceiich.24485691e.2012.1.45167

[25] Ong, C. B., Ng, L. Y., Mohammad, A. W. "A review of ZnO nanoparticles as solar photocatalysts: Synthesis, mechanisms and applications", Renewable and Sustainable Energy Reviews, 81(1), pp. 536–551, 2018.
https://doi.org/10.1016/j.rser.2017.08.020

[26] Dehghanghadikolaei, A., Ansary, J., Ghoreishi, R. "Sol-gel process applications: A mini-review", Proceedings of the Nature Research Society, 2, pp. 1–11, 2018.
https://doi.org/10.11605/j.pnrs.201802008

[27] Akpan, U. G., Hameed, B. H. "Parameters affecting the photocatalytic degradation of dyes using TiO_2-based photocatalysts: A review", Journal of Hazardous Materials, 170(2–3), pp. 520–529, 2009.
https://doi.org/10.1016/j.jhazmat.2009.05.039

[28] Pelaez, M., Nolan, N. T., Pillai, S. C., Seery, M. K., Falaras, P., Kontos, A. G., Dunlop, P. S. M., Hamilton, J. W. J., Byrne, J. A., O'Shea, K., Entezari, M. H., Dionysiou, D. D. "A review on the visible light active titanium dioxide photocatalysts for environmental applications", Applied Catalysis B: Environmental, 125, pp. 331–349, 2012.
https://doi.org/10.1016/j.apcatb.2012.05.036

[29] Lee, K. M., Lai, C. W., Ngai, K. S., Juan, J. C. "Recent developments of zinc oxide based photocatalyst in water treatment technology: A review", Water Research, 88(1), pp. 428–448, 2016.
https://doi.org/10.1016/j.watres.2015.09.045

[30] Nisansala Bandara, W. R. L., De Silva, R. M., De Silva, K. M. N., Dahanayake, D., Gunasekara, S., Thanabalasingam, K. "Is nano ZrO_2 a better photocatalyst than nano TiO_2 for degradation of plastics?", RSC Advances, 7(73), pp. 46155–46163, 2017.
https://doi.org/10.1039/c7ra08324f

[31] Basahel, S. N., Ali, T. T., Mokhtar, M., Narasimharao, K. "Influence of crystal structure of nanosized ZrO_2 on photocatalytic degradation of methyl orange", Nanoscale Research Letters, 10(1), Article number: 73, 2015.
https://doi.org/10.1186/s11671-015-0780-z

[32] Lachheb, H., Puzenat, E., Houas, A., Ksibi, M., Elaloui, E., Guillard, C., Herrmann, J. M. "Photocatalytic degradation of various types of dyes (Alizarin S, Crocein Orange G, Methyl Red, Congo Red, Methylene Blue) in water by UV-irradiated titania", Applied Catalysis B: Environmental, 39(1), pp. 75–90, 2002.
https://doi.org/10.1016/S0926-3373(02)00078-4

[33] Sathiyan, K., Bar-Ziv, R., Mendelson, O., Zidki, T. "Controllable synthesis of TiO_2 nanoparticles and their photocatalytic activity in dye degradation", Materials Research Bulletin, 126, Article number: 110842, 2020.
https://doi.org/10.1016/j.materresbull.2020.110842

[34] Jamil, A., Bokhari, T. H., Javed, T., Mustafa, R., Sajid, M., Noreen, S., Zuber, M., Nazir, A., Iqbal, M., Jilani, M. I. "Photocatalytic degradation of disperse dye Violet-26 using TiO_2 and ZnO nanomaterials and process variable optimization", Journal of Materials Research and Technology, 9(1), pp. 1119–1128, 2020.
https://doi.org/10.1016/j.jmrt.2019.11.035

[35] Ammari, Y., El Atmani, K., Bay, L., Bakas, I., Qourzal, S., Ait Ichou, I. "Elimination of a mixture of two dyes by photocatalytic degradation based on TiO_2 P-25 Degussa", Materials Today Proceedings, 22(1), pp. 126–129, 2020.
https://doi.org/10.1016/j.matpr.2019.08.142

[36] Hu, H., Lin, Y., Hu, Y. H. "Core-shell structured TiO_2 as highly efficient visible light photocatalyst for dye degradation", Catalysis Today, 341, pp. 90–95, 2020.
https://doi.org/10.1016/j.cattod.2019.01.077

[37] Li, X., Yang, H., Lv, K., Wen, L., Liu, Y. "Fabrication of porous TiO_2 nanosheets assembly for improved photoreactivity towards X3B dye degradation and NO oxidation", Applied Surface Science, 503, Article number: 144080, 2020.
https://doi.org/10.1016/j.apsusc.2019.144080

[38] Hanafi, M. F., Sapawe, N. "The Potential of ZrO_2 Catalyst Toward Degradation of Dyes and Phenolic Compound", Materials Today Proceedings, 19(4), pp. 1524–1528, 2019.
https://doi.org/10.1016/j.matpr.2019.11.177

[39] Mansouri, M., Mozafari, N., Bayati, B., Setareshenas, N. "Photocatalytic dye degradation of methyl orange using zirconia – zeolite nanoparticles", Bulletin of Materials Science, 42(5), Article number: 230, 2019.
https://doi.org/10.1007/s12034-019-1933-y

[40] Rodrigues, J., Hatami, T., Rosa, J. M., Tambourgi, E. B., Mei, L. H. I. "Photocatalytic degradation using ZnO for the treatment of RB 19 and RB 21 dyes in industrial effluents and mathematical modeling of the process", Chemical Engineering Research and Design, 153, pp. 294–305, 2020.
https://doi.org/10.1016/j.cherd.2019.10.021

[41] Satdeve, N. S., Ugwekar, R. P., Bhanvase, B. A. "Ultrasound assisted preparation and characterization of Ag supported on ZnO nanoparticles for visible light degradation of methylene blue dye", Journal of Molecular Liquids, 291, Article number: 111313, 2019.
https://doi.org/10.1016/j.molliq.2019.111313

[42] Chijioke-Okere, M. O., Okorocha, N. J., Anukam, B. N., Oguzie, E. E. "Photocatalytic Degradation of a Basic Dye Using Zinc Oxide Nanocatalyst", International Letters of Chemistry, Physics, and Astronomy, 81, pp. 18–26, 2019.
https://doi.org/10.18052/www.scipress.com/ilcpa.81.18

[43] Bagheri, M., Najafabadi, N. R., Borna, E. "Removal of reactive blue 203 dye photocatalytic using ZnO nanoparticles stabilized on functionalized MWCNTs", Journal of King Saud University - Science, 32(1), pp. 799–804, 2020.
https://doi.org/10.1016/j.jksus.2019.02.012

[44] Chen, X., Wu, Z., Liu, D., Gao, Z. "Preparation of ZnO Photocatalyst for the Efficient and Rapid Photocatalytic Degradation of Azo Dyes", Nanoscale Research Letters, 12(1), Article number: 143, 2017.
https://doi.org/10.1186/s11671-017-1904-4

[45] Wang, X., Long, R., Liu, D., Yang, D., Wang, C., Xiong, Y. "Enhanced full-spectrum water splitting by confining plasmonic Au nanoparticles in N-doped TiO_2 bowl nanoarrays", Nano Energy, 24, pp. 87–93, 2016.
https://doi.org/10.1016/j.nanoen.2016.04.013

[46] Pirzada, B. M., Mir, N. A., Qutub, N., Mehraj, O., Sabir, S., Muneer, M. "Synthesis, characterization, and optimization of photocatalytic activity of TiO_2/ZrO_2 nanocomposite heterostructures", Materials Science and Engineering: B, 193, pp. 137–145, 2015.
https://doi.org/10.1016/j.mseb.2014.12.005

[47] Periyannan, S., Manceriu, L., Nguyen, N. D., Klein, A., Jaegermann, W., Colson, P., Henrist, C., Cloots, R. "Influence of ZnO Surface Modification on the Photocatalytic Performance of ZnO/NiO Thin Films", Catalysis Letters, 149(7), pp. 1813–1824, 2019.
https://doi.org/10.1007/s10562-019-02781-z

[48] Parul, Kaur, K., Badru, R., Singh, P. P., Kaushal, S. "Photodegradation of organic pollutants using heterojunctions: A review", Journal of Environmental Chemical Engineering, 8(2), Article number: 103666, 2020.
https://doi.org/10.1016/j.jece.2020.103666

[49] Low, J., Yu, J., Jaroniec, M., Wageh, S., Al-Ghamdi, A. A. "Heterojunction Photocatalysts", Advanced Materials, 29(20), Article number: 1601694, 2017.
https://doi.org/10.1002/adma.201601694

[50] Zhu, Y., Wan, T., Wen, X., Chu, D., Jiang, Y. "Tunable Type I and II heterojunction of CoO_x nanoparticles confined in g-C_3N_4 nanotubes for photocatalytic hydrogen production", Applied Catalysis B: Environmental, 244, pp. 814–822, 2019.
https://doi.org/10.1016/j.apcatb.2018.12.015

[51] Moniz, S. J. A., Shevlin, S. A., Martin, D. J., Guo, Z. X., Tang, J. "Visible-light driven heterojunction photocatalysts for water splitting - a critical review", Energy & Environmental Science, 8(3), pp. 731–759, 2015.
https://doi.org/10.1039/c4ee03271c

[52] Chen, W., Liu, T. Y., Huang, T., Liu, X. H., Duan, G. R., Yang, X. J., Chen, S. M. "A novel yet simple strategy to fabricate visible light responsive C,N-TiO_2/g-C_3N_4 heterostructures with significantly enhanced photocatalytic hydrogen generation", RSC Advances, 5(122), pp. 101214–101220, 2015.
https://doi.org/10.1039/c5ra18302b

[53] Prabhu, S., Pudukudy, M., Harish, S., Navaneethan, M., Sohila, S., Murugesan, K., Ramesh, R. "Facile construction of djembe-like ZnO and its composite with g-C_3N_4 as a visible-light-driven heterojunction photocatalyst for the degradation of organic dyes", Materials Science in Semiconductor Processing, 106, Article number: 104754, 2020.
https://doi.org/10.1016/j.mssp.2019.104754

[54] Ramezanalizadeh, H., Rafiee, E. "Design, fabrication, electro- and photoelectrochemical investigations of novel $CoTiO_3/CuBi_2O_4$ heterojunction semiconductor: An efficient photocatalyst for the degradation of DR16 dye", Materials Science and Semiconductor Processing, 113, Article number: 105055, 2020.
https://doi.org/10.1016/j.mssp.2020.105055

[55] Chen, Y., Qian, J., Wang, N., Xing, J., Liu, L. "In-situ synthesis of CNT/TiO_2 heterojunction nanocomposite and its efficient photocatalytic degradation of Rhodamine B dye", Inorganic Chemistry Communications, 119, Article number: 108071, 2020.
https://doi.org/10.1016/j.inoche.2020.108071

[56] Chen, C. J., Liao, C. H., Hsu, K. C., Wu, Y. T., Wu, J. C. S. "P-N junction mechanism on improved NiO/TiO_2 photocatalyst", Catalysis Communications, 12(14), pp. 1307–1310, 2011.
https://doi.org/10.1016/j.catcom.2011.05.009

[57] Cao, J., Li, X., Lin, H., Chen, S., Fu, X. "In situ preparation of novel p-n junction photocatalyst BiOI/$(BiO)_2CO_3$ with enhanced visible light photocatalytic activity", Journal of Hazardous Materials, 239–240, pp. 316–324, 2012.
https://doi.org/10.1016/j.jhazmat.2012.08.078

[58] Xu, J., Feng, B., Wang, Y., Qi, Y., Niu, J., Chen, M. "BiOCl Decorated $NaNbO_3$ Nanocubes: A Novel p-n Heterojunction Photocatalyst With Improved Activity for Ofloxacin Degradation", Frontiers in Chemistry, 6, Article number: 393, 2018.
https://doi.org/10.3389/fchem.2018.00393

[59] Habibi-Yangjeh, A., Pirhashemi, M., Ghosh, S. "ZnO/$ZnBi_2O_4$ nanocomposites with p-n heterojunction as durable visible-light-activated photocatalysts for efficient removal of organic pollutants", Journal of Alloys Compounds, 826, Article number: 154229, 2020.
https://doi.org/10.1016/j.jallcom.2020.154229

[60] Sang, Y., Cao, X., Dai, G., Wang, L., Peng, Y., Geng, B. "Facile one-pot synthesis of novel hierarchical Bi_2O_3/Bi_2S_3 nanoflower photocatalyst with intrinsic p-n junction for efficient photocatalytic removals of RhB and Cr(VI)", Journal of Hazardous Materials, 381, Article number: 120942, 2020.
https://doi.org/10.1016/j.jhazmat.2019.120942

[61] Lu, X., Li, Q., Liu, S., Luo, R., Li, H., Zhang, M., Cui, C., Zhu, G., Chen, S., Liang, C. "Fabrication of a novel BiOI/KTaO$_3$ p–n heterostructure with enhanced photocatalytic performance under visible-light irradiation", RSC Advances, 10(18), pp. 10921–10931, 2020.
https://doi.org/10.1039/c9ra10231k

[62] Yu, J., Wang, S., Low, J., Xiao, W. "Enhanced photocatalytic performance of direct Z-scheme g-C$_3$N$_4$/TiO$_2$ photocatalyst for decomposition of formaldehyde in air", Physical Chemistry Chemical Physics, 15(39), pp. 16883–16890, 2013.
https://doi.org/https://doi.org/10.1039/C3CP53131G

[63] Qi, K., Cheng, B., Yu, J., Ho, W. "A review on TiO$_2$-based Z-scheme photocatalysts", Chinese Journal of Catalysis, 38(12), pp. 1936–1955, 2017.
https://doi.org/10.1016/S1872-2067(17)62962-0

[64] Low, J., Jiang, C., Cheng, B., Wageh, S., Al-Ghamdi, A. A., Yu, J. "A Review of Direct Z-Scheme Photocatalysts", Small Methods, 1(5), Article number: 1700080, 2017.
https://doi.org/10.1002/smtd.201700080

[65] Xu, Q., Zhang, L., Yu, J., Wageh, S., Al-Ghamdi, A. A., Jaroniec, M. "Direct Z-scheme photocatalysts: Principles, synthesis, and applications", Materials Today, 21(10), pp. 1042–1063, 2018.
https://doi.org/10.1016/j.mattod.2018.04.008

[66] Zhao, J, Ji, M., Di, J, Zhang, Y., He, M., Li, H., Xia, J. "Novel Z-scheme heterogeneous photo-Fenton-like g-C$_3$N$_4$/FeOCl for the pollutants degradation under visible light irradiation", Journal of Photochemistry and Photobiology A: Chemistry, 391, Article number: 112343, 2020.
https://doi.org/10.1016/j.jphotochem.2019.112343

[67] An, W., Sun, K., Hu, J., Cui, W., Liu, L. "The Z-scheme Ag$_2$CO$_3$@g-C$_3$N$_4$ core-shell structure for increased photoinduced charge separation and stable photocatalytic degradation", Applied Surface Science, 504, Article number: 144345, 2020.
https://doi.org/10.1016/j.apsusc.2019.144345

[68] Zhang, T., Wang, X., Sun, Z., Liang, Q., Zhou, M., Xu, S., Li, Z., Sun, D. "Constructing Z-scheme based BiOI/CdS heterojunction with efficient visible-light photocatalytic dye degradation", Solid State Science, 107, Article number: 106350, 2020.
https://doi.org/10.1016/j.solidstatesciences.2020.106350

[69] Masih, D., Ma, Y., Rohani, S. "Graphitic C$_3$N$_4$ based noble-metal-free photocatalyst systems: A review", Applied Catalysis B: Environmental, 206, pp. 556–588, 2017.
https://doi.org/10.1016/j.apcatb.2017.01.061

[70] Ye, L., Liu, J., Jiang, Z., Peng, T., Zan, L. "Facets coupling of BiOBr-g-C$_3$N$_4$ composite photocatalyst for enhanced visible-light-driven photocatalytic activity", Applied Catalysis B: Environmental, 142–143, pp. 1–7, 2013.
https://doi.org/10.1016/j.apcatb.2013.04.058

[71] Wei, X., Liu, H., Li, T., Jiang, Z., Hu, W., Niu, Q., Chen, J. "Three-dimensional flower heterojunction g-C$_3$N$_4$/Ag/ZnO composed of ultrathin nanosheets with enhanced photocatalytic performance", Journal of Photochemistry and Photobiology A: Chemistry, 390, Article number: 112342, 2020.
https://doi.org/10.1016/j.jphotochem.2019.112342

[72] Zhao, X., Zhang, X., Han, D., Niu, L. "Ag supported Z-scheme WO$_{2.9}$/g-C$_3$N$_4$ composite photocatalyst for photocatalytic degradation under visible light", Applied Surface Science, 501, Article number: 144258, 2020.
https://doi.org/10.1016/j.apsusc.2019.144258

[73] Xue, S., Wu, C., Pu, S., Hou, Y., Tong, T., Yang, G., Qin, Z., Wang, Z., Bao, J. "Direct Z-Scheme charge transfer in heterostructured MoO$_3$/g-C$_3$N$_4$ photocatalysts and the generation of active radicals in photocatalytic dye degradations", Environmental Pollution, 250, pp. 338–345, 2019.
https://doi.org/10.1016/j.envpol.2019.04.010

[74] Hu, C., Huang, H. X., Lin, Y. F., Yoshida, M., Chen, T. H. "Decoration of SrTiO$_3$ nanofibers by BiOI for photocatalytic methyl orange degradation under visible light irradiation", Journal of the Taiwan Institute of Chemical Engineers, 96, pp. 264–272, 2019.
https://doi.org/10.1016/j.jtice.2018.11.020

[75] Ren, B., Shen, W., Li, L., Wu, S., Wang, W. "3D CoFe$_2$O$_4$ nanorod/flower-like MoS$_2$ nanosheet heterojunctions as recyclable visible light-driven photocatalysts for the degradation of organic dyes", Applied Surface Science, 447, pp. 711–723, 2018.
https://doi.org/10.1016/j.apsusc.2018.04.064

[76] Qin, J., Chen, N., Feng, C., Chen, H., Feng, Z., Gao, Y., Zhang, Z. "Fabrication of a Novel p–n Heterojunction BiOCl/Ag$_6$Si$_2$O$_7$ Nanocomposite as a Highly Efficient and Stable Visible Light Driven Photocatalyst", Catalysis Letters, 149(3), pp. 891–903, 2019.
https://doi.org/10.1007/s10562-018-2631-x

[77] Jia, K. L., Zhu, Z. S., Qu, J., Jing, Y. Q., Yu, X. J., Abdelkrim, Y., Hao, S. M., Yu, Z. Z. "BiOBr/Ag$_6$Si$_2$O$_7$ heterojunctions for enhancing visible light catalytic degradation performances with a sequential selectivity enabled by dual synergistic effects", Journal of Colloid and Interface Science, 561, pp. 396–407, 2020.
https://doi.org/10.1016/j.jcis.2019.11.005

[78] Ramezanalizadeh, H., Manteghi, F. "Design and development of a novel BiFeO$_3$/CuWO$_4$ heterojunction with enhanced photocatalytic performance for the degradation of organic dyes", Journal of Photochemistry and Photobiology A: Chemistry, 338, pp. 60–71, 2017.
https://doi.org/10.1016/j.jphotochem.2017.02.004

[79] Ding, M., Zhou, J., Yang, H., Cao, R., Zhang, S., Shao, M., Xu, X. "Synthesis of Z-scheme g-C$_3$N$_4$ nanosheets/Ag$_3$PO$_4$ photocatalysts with enhanced visible-light photocatalytic performance for the degradation of tetracycline and dye", Chinese Chemical Letters, 31(1), pp. 71–76, 2020.
https://doi.org/10.1016/j.cclet.2019.05.029

[80] Yan, Y., Yang, M., Wang, C., Liu, E., Hu, X., Fan, J. "Defected ZnS/bulk g–C$_3$N$_4$ heterojunction with enhanced photocatalytic activity for dyes oxidation and Cr (VI) reduction", Colloids and Surfaces A: Physicochemical and Engineering Aspects, 582, Article number: 123861, 2019.
https://doi.org/10.1016/j.colsurfa.2019.123861

[81] Zhang, H., Yu, D., Wang, W., Gao, P., Bu, K., Zhang, L., Zhong, S., Liu, B. "Multiple heterojunction system of Bi_2MoO_6/ WO_3/Ag_3PO_4 with enhanced visible-light photocatalytic performance towards dye degradation", Advanced Powder Technology, 30(9), pp. 1910–1919, 2019.
https://doi.org/10.1016/j.apt.2019.06.010

[82] Yang, F., Yan, L., Zhang, B., He, X., Li, Y., Tang, Y., Ma, C., Li, Y. "Fabrication of ternary $NaTaO_3$/g-C_3N_4/G heterojunction photocatalyst with enhanced activity for Rhodamine B degradation", Journal of Alloys Compounds, 805, pp. 802–810, 2019.
https://doi.org/10.1016/j.jallcom.2019.07.052

[83] Kang, M. J., Yu, H., Lee, W., Cha, H. G. "Efficient Fe_2O_3 /C-g-C_3N_4 Z-scheme heterojunction photocatalyst prepared by facile one-step carbonizing process", Journal of Physics and Chemistry Solids, 130, pp. 93–99, 2019.
https://doi.org/10.1016/j.jpcs.2019.02.017

[84] Huang, H., He, M., Yang, X., Tian, Z., Hu, J., Wen, B. "One-pot hydrothermal synthesis of TiO_2/RCN heterojunction photocatalyst for production of hydrogen and rhodamine B degradation", Appllied Surface Science, 493, pp. 202–211, 2019.
https://doi.org/10.1016/j.apsusc.2019.07.013

[85] Kaviyarasu, K., Maria Magdalane, C., Jayakumar, D., Samson, Y., Bashir, A. K. H., Maaza, M., Letsholathebe, D., Mahmoud, A. H., Kennedy, J. "High performance of pyrochlore like $Sm_2Ti_2O_7$ heterojunction photocatalyst for efficient degradation of rhodamine-B dye with waste water under visible light irradiation", Journal of King Saud University – Science, 32(2), pp. 1516–1522, 2020.
https://doi.org/10.1016/j.jksus.2019.12.006

[86] Dashairya, L., Mehta, A., Saha, P., Basu, S. "Visible-light-induced enhanced photocatalytic degradation of Rhodamine-B dye using $Bi_xSb_{2-x}S_3$ solid-solution photocatalysts", Journal of Colloid Interface Science, 561, pp. 71–82, 2020.
https://doi.org/10.1016/j.jcis.2019.11.118

[87] Bera, K. K., Chakraborty, M., Mondal, M., Banik, S., Bhattacharya, S. K. "Synthesis of α-β Bi_2O_3 heterojunction photocatalyst and evaluation of reaction mechanism for degradation of RhB dye under natural sunlight", Ceramics International, 46(6), pp. 7667–7680, 2020.
https://doi.org/10.1016/j.ceramint.2019.11.269

[88] Li, N., Miao, S., Zheng, X., Lai, J., Lv, S., Gu, X., Zhang, M., Yang, J., Cui, S. "Construction of Ag_3PO_4/$BiNbO_4$ heterojunction photocatalysts with high activity for Rhodamine B removal under simulated sunlight irradiation", Ceramics International, 45(18), pp. 24260–24268, 2019.
https://doi.org/10.1016/j.ceramint.2019.08.138

[89] Hu, X., Wang, G., Wang, J., Hu, Z., Su, Y. "Step-scheme NiO/BiOI heterojunction photocatalyst for rhodamine photodegradation", Applied Surface Science, 511, Article number: 145499, 2020.
https://doi.org/10.1016/j.apsusc.2020.145499

[90] Zeynali, S., Taghizadeh, M. T. "Highly efficient TiO_2/AgBr/PANI heterojunction with enhanced visible light photocatalytic activity towards degradation of organic dyes", Journal of Materials Science: Materials in Electronics, 30(18), pp. 17020–17031, 2019.
https://doi.org/10.1007/s10854-019-02036-y

[91] Sajid, M. M., Shad, N. A., Javed, Y., Khan, S. B., Amin, N., Zhang, Z., Imran, Z., Yousuf, M. I. "Facile synthesis of $Zn_3(VO_4)_2$/ $FeVO_4$ heterojunction and study on its photocatalytic and electrochemical properties", Applied Nanoscience, 10(7), pp. 421–433, 2020.
https://doi.org/10.1007/s13204-019-01199-8

[92] Wu, K., Qin, Z., Zhang, X., Guo, R., Ren, X., Pu, X. "Z-scheme $BiOCl$/Bi–Bi_2O_3 heterojunction with oxygen vacancy for excellent degradation performance of antibiotics and dyes", Journal of Materials Science, 55(9), pp. 4017–4029, 2020.
https://doi.org/10.1007/s10853-019-04300-2

[93] Jiang, T., Wang, K., Guo, T., Wu, X., Zhang, G. "Fabrication of Z-scheme MoO_3/Bi_2O_4 heterojunction photocatalyst with enhanced photocatalytic performance under visible light irradiation", Chinese Journal of Catalysis, 41(1), pp. 161–169, 2020.
https://doi.org/10.1016/S1872-2067(19)63391-7

[94] Lakhera, S. K., Venkataramana, R., Mathew, G., Hafeez, H. Y., Neppolian, B. "Fabrication of high surface area AgI incorporated porous $BiVO_4$ heterojunction photocatalysts", Materials Science In Semiconductor Processing, 106, Article number: 104756, 2020.
https://doi.org/10.1016/j.mssp.2019.104756

[95] Wang, X., Ma, J., Kong, Y., Fan, C., Peng, M., Komarneni, S. "Synthesis of p-n heterojunction Ag_3PO_4/$NaTaO_3$ composite photocatalyst for enhanced visible-light-driven photocatalytic performance", Materials Letters, 251, pp. 192–195, 2019.
https://doi.org/10.1016/j.matlet.2019.05.078

[96] Assayehegn, E., Solaiappan, A., Chebude, Y., Alemayehu, E. "Fabrication of tunable anatase/rutile heterojunction N/TiO_2 nanophotocatalyst for enhanced visible light degradation activity", Applied Surface Science, 515, Article number: 145966, 2020.
https://doi.org/10.1016/j.apsusc.2020.145966

[97] Cao, X., Chen, Y., Jiao, S., Fang, Z., Xu, M., Liu, X., Li, L., Pang, G., Feng, S. "Magnetic photocatalysts with a p-n junction: Fe_3O_4 nanoparticle and $FeWO_4$ nanowire heterostructures", Nanoscale, 6(21), pp. 12366–12370, 2014.
https://doi.org/10.1039/c4nr03729d

[98] Chen, J., Wang, M., Han, J., Guo, R. "TiO_2 nanosheet/NiO nanorod hierarchical nanostructures: p–n heterojunctions towards efficient photocatalysis", Journal of Colloid Interface Science, 562, pp. 313–321, 2020.
https://doi.org/10.1016/j.jcis.2019.12.031

[99] Ayappan, C., Palanivel, B., Jayaraman, V., Maiyalagan, T., Mani, A. "One-step hydrothermal synthesis of $CaWO_4$/α-Ag_2WO_4 heterojunction: An efficient photocatalyst for removal of organic contaminants", Materials Science in Semiconductor Processing, 104, Article number: 104693, 2019.
https://doi.org/10.1016/j.mssp.2019.104693

[100] Nithya, M., Vidhya, S., Keerthi. "A novel g-C_3N_4/MnV_2O_6 heterojunction photocatalyst for the removal of methylene blue and indigo carmine", Chemical Physics Letters, 737, Article number: 136832, 2019.
https://doi.org/10.1016/j.cplett.2019.136832

[101] Zhang, R., Zhang, T., Zhao, C., Han, Q., Li, Y., Liu, Y., Zeng, K. "A novel Z-scheme Bi_2WO_6 -based photocatalyst with enhanced dye degradation activity", Journal of Nanoparticle Research, 21(9), Article number: 203, 2019.
https://doi.org/10.1007/s11051-019-4652-9

[102] Qi, S., Wang, D., Zhao, Y., Xu, H. "Core–shell g-$C_3N_4@Zn_{0.5}Cd_{0.5}S$ heterojunction photocatalysts with high photocatalytic activity for the degradation of organic dyes", Journal of Materials Science: Materials in Electronics, 30(5), pp. 5284–5296, 2019.
https://doi.org/10.1007/s10854-019-00828-w

[103] Rizal, M. Y., Saleh, R., Taufik, A. "Characterization and photocatalytic activity of Ag/Mn_3O_4/graphene composites under visible light irradiation for organic dyes degradation", Journal of Environmental Chemical Engineering, 8(3), Article number: 103610, 2020.
https://doi.org/10.1016/j.jece.2019.103610

[104] Venkataswamy, P., Sudheera, M., Vaishnavi, K., Ramaswamy, K., Ravi, G., Vithal, M. "A New $Ag/AgBr/LaAlO_3$ Plasmonic Composite: Synthesis, Characterization, and Visible-Light Driven Photocatalytic Activity", Journal of Electronics Materials, 49(4), pp. 2358–2370, 2020.
https://doi.org/10.1007/s11664-019-07938-5

[105] Zhu, J., He, J., Hu, L. "A novel $Cu_2O@HNbWO_6$ heterojunction photocatalyst with enhanced photocatalytic performance", Materials Letters, 254, pp. 297–300, 2019.
https://doi.org/10.1016/j.matlet.2019.07.062

[106] Hasija, V., Raizada, P., Sudhaik, A., Singh, P., Thakur, V. K., Khan, A. A. P. "Fabrication of $Ag/AgI/WO_3$ heterojunction anchored P and S co-doped graphitic carbon nitride as a dual Z scheme photocatalyst for efficient dye degradation", Solid State Science, 100, Article number: 106095, 2020.
https://doi.org/10.1016/j.solidstatesciences.2019.106095

[107] Cui, H., Li, B., Li, Z., Li, X., Xu, S. "Z-scheme based $CdS/CdWO_4$ heterojunction visible light photocatalyst for dye degradation and hydrogen evolution", Applied Surface Science, 455, pp. 831–840, 2018.
https://doi.org/10.1016/j.apsusc.2018.06.054

[108] Chen, X., He, X., Yang, X., Wu, Z., Li, Y. "Construction of novel 2D/1D g-$C_3N_4/CaTiO_3$ heterojunction with face-to-face contact for boosting photodegradation of triphenylmethane dyes under simulated sunlight", Journal of the Taiwan Institute of Chemical Engineers, 107, pp. 98–109, 2020.
https://doi.org/10.1016/j.jtice.2019.12.002

[109] Mafa, P. J., Ntsendwana, B., Mamba, B. B., Kuvarega, A. T. "Visible Light Driven $ZnMoO_4/BiFeWO_6$/rGO Z-Scheme Photocatalyst for the Degradation of Anthraquinonic Dye", Journal of Physical Chemistry C, 123(33), pp. 20605–20616, 2019.
https://doi.org/10.1021/acs.jpcc.9b05008

[110] Solehudin, M., Sirimahachai, U., Ali, G. A. M., Chong, K. F., Wongnawa, S. "One-pot synthesis of isotype heterojunction g-C_3N_4-MU photocatalyst for effective tetracycline hydrochloride antibiotic and reactive orange 16 dye removal", Advanced Powder Technology, 31(5), pp. 1891–1902, 2020.
https://doi.org/10.1016/j.apt.2020.02.020

[111] Wei, X., Xu, X., Yang, X., Li, J., Liu, Z. "Visible light degradation of reactive black-42 by novel Sr/Ag-$TiO_2@g$-C_3N_4 photocatalyst: RSM optimization, reaction kinetics and pathways", Spectrochimica Acta Part A: Molecular and Biomolecular Spectroscopy, 228, Article number: 117870, 2020.
https://doi.org/10.1016/j.saa.2019.117870

[112] Fei, W., Li, H., Li, N., Chen, D., Xu, Q., Li, H., He, J., Lu, J. "Facile fabrication of ZnO/MoS_2 p-n junctions on Ni foam for efficient degradation of organic pollutants through photoelectrocatalytic process", Solar Energy, 199, pp. 164–172, 2020.
https://doi.org/10.1016/j.solener.2020.02.037

[113] Wang, Y., Tian, H. "Study on the construction of $YMnO_3/CeO_2$ composite photocatalyst heterostructure and photocatalytic degradation of methyl red", Optik, 201, Article number: 163524, 2020.
https://doi.org/10.1016/j.ijleo.2019.163524

[114] Akbarzadeh, E., Soheili, H. Z., Hosseinifard, M., Gholami, M. R. "Preparation and characterization of novel Ag_3VO_4/Cu-MOF/rGO heterojunction for photocatalytic degradation of organic pollutants", Materials Research Bulletin, 121, Article number: 110621, 2020.
https://doi.org/10.1016/j.materresbull.2019.110621

[115] Di, L., Yang, H., Xian, T., Chen, X. "Facile Synthesis and Enhanced Visible-Light Photocatalytic Activity of Novel p-Ag_3PO_4/n-$BiFeO_3$ Heterojunction Composites for Dye Degradation", Nanoscale Research Letters, 13(1), Article number: 257, 2018.
https://doi.org/10.1186/s11671-018-2671-6

[116] Escobar-Villanueva, A. G., Ovando-Medina, V. M., Martínez-Gutiérrez, H., Militello, M. P. "Fast photodegradation of Orange II azo dye under visible light irradiation using a semiconducting n–p heterojunction of ZnO nanoparticles/polypyrrole as catalyst", Journal of Materials Science: Materials in Electronics, 31(2), pp. 1317–1327, 2020.
https://doi.org/10.1007/s10854-019-02644-8

[117] Yang, R., Zhao, Q., Liu, B. "Two-step method to prepare the direct Z-scheme heterojunction hierarchical flower-like $Ag@AgBr/Bi_2MoO_6$ microsphere photocatalysts for waste water treatment under visible light", Journal of Materials Science: Materials in Electronics, 31(7), pp. 5054–5067, 2020.
https://doi.org/10.1007/s10854-020-03040-3

[118] Ritika, Kaur, M., Umar, A., Mehta, S. K., Kansal, S. K., Khan, M. A., Algarni, H. "Enhanced solar light-mediated photocatalytic degradation of brilliant green dye in aqueous phase using $BiPO_4$ nanospindles and $MoS_2/BiPO_4$ nanorods", Journal of Materials Science Materials in Electronics, 30(23), pp. 20741–20750, 2019.
https://doi.org/10.1007/s10854-019-02441-3

[119] Dijkstra, M. F. J., Michorius, A., Buwalda, H., Panneman, H. J., Winkelman, J. G. M., Beenackers, A. A. C. M. "Comparison of the efficiency of immobilized and suspended systems in photocatalytic degradation", Catalysis Today, 66(2–4), pp. 487–494, 2001.
https://doi.org/10.1016/S0920-5861(01)00257-7

[120] Padoin, N., Soares, C. "An explicit correlation for optimal TiO_2 film thickness in immobilized photocatalytic reaction systems", Chemical Engineering Journal, 310(2), pp. 381–388, 2017.
https://doi.org/10.1016/j.cej.2016.06.013

[121] Bahrudin, N. N., Nawi, M. A. "Mechanistic of photocatalytic decolorization and mineralization of methyl orange dye by immobilized TiO_2/chitosan-montmorillonite", Journal of Water Process Engineering, 31, Article number: 100843, 2019.
https://doi.org/10.1016/j.jwpe.2019.100843

[122] Ounas, O., El Foulani, A. A., Lekhlif, B., Jamal-Eddine, J. "Immobilization of TiO_2 into a poly methyl methacrylate (PMMA) as hybrid film for photocatalytic degradation of methylene blue", Materials Today: Proceedings, 22(1), pp. 35–40, 2020.
https://doi.org/10.1016/j.matpr.2019.08.068

[123] de Araujo Scharnberg, A. R., de Loreto, A. C., Wermuth, T. B., Alves, A. K., Arcaro, S., dos Santos, P. A. M., de Assis Lawisch Rodriguez, A. "Porous ceramic supported TiO_2 nanoparticles: Enhanced photocatalytic activity for Rhodamine B degradation", Boletín de La Sociedad Española de Cerámica y Vidrio, 59(6), pp. 230–238, 2020.
https://doi.org/10.1016/j.bsecv.2019.12.001

[124] Inderyas, A., Bhatti, I. A., Ashar, A., Ashraf, M., Ghani, A., Yousaf, M., Mohsin, M., Ahmad, M., Rafique, S., Masood, N., Iqbal, M. "Synthesis of immobilized ZnO over polyurethane and photocatalytic activity evaluation for the degradation of azo dye under UV and solar light irradiation", Materials Research Express, 7(2), Article number: 025033, 2020.
https://doi.org/10.1088/2053-1591/ab715f

[125] Das, S., Mahalingam, H. "Novel immobilized ternary photocatalytic polymer film based airlift reactor for efficient degradation of complex phthalocyanine dye wastewater", Journal of Hazardous Materials, 383, Article number: 121219, 2020.
https://doi.org/10.1016/j.jhazmat.2019.121219

[126] Hir, Z. A. M., Moradihamedani, P., Abdullah, A. H., Mohamed, M. A. "Immobilization of TiO_2 into polyethersulfone matrix as hybrid film photocatalyst for effective degradation of methyl orange dye", Materials Science in Semiconductor Processing, 57, pp. 157–165, 2020.
https://doi.org/10.1016/j.mssp.2016.10.009

[127] Ramezanalizadeh, H., Zakeri, F., Manteghi, F. "Immobilization of $BaWO_4$ nanostructures on a MOF-199-NH_2: An efficient separable photocatalyst for the degradation of organic dyes", Optik, 174, pp. 776–786, 2018.
https://doi.org/10.1016/j.ijleo.2018.08.052

[128] Ahmed, S. N., Inam, A., Haider, W. "γ-Fe_2O_3 photocatalyst immobilized on a porous Ni substrate for recyclable solar photocatalysis", Journal of Nanoparticle Research, 21(11), Article number: 238, 2019.
https://doi.org/10.1007/s11051-019-4663-6

[129] Khalilian, H., Behpour, M., Atouf, V., Hosseini, S. N. "Immobilization of S, N-codoped TiO_2 nanoparticles on glass beads for photocatalytic degradation of methyl orange by fixed bed photoreactor under visible and sunlight irradiation", Solar Energy, 112, pp. 239–245, 2015.
https://doi.org/10.1016/j.solener.2014.12.007

[130] Arikal, D., Kallingal, A. "Photocatalytic degradation of azo and anthraquinone dye using TiO_2/MgO nanocomposite immobilized chitosan hydrogels", Environmental Technology, 42(15), pp. 2278–2291, 2021.
https://doi.org/10.1080/09593330.2019.1701094

[131] Yu, Y., Zhu, X., Wang, L., Wu, F., Liu, S., Chang, C., Luo, X. "A simple strategy to design 3-layered Au-TiO_2 dual nanoparticles immobilized cellulose membranes with enhanced photocatalytic activity", Carbohydrate Polymers, 231, Article number: 115694, 2020.
https://doi.org/10.1016/j.carbpol.2019.115694

[132] Zhang, X., Li, R., Wang, Y., Zhang, X., Wang, Y., Fan, C. "Slow-releasing Cl^- to prepare BiOCl thin film on Bi plate and its photocatalytic properties", Materials Letters, 174, pp. 126–128, 2016.
https://doi.org/10.1016/j.matlet.2016.03.109

[133] Wang, B., de Godoi, F.C., Sun, Z., Zeng, Q., Zheng, S., Frost, R. L. "Synthesis, characterization and activity of an immobilized photocatalyst: Natural porous diatomite supported titania nanoparticles", Journal of Colloid Interface Science, 438, pp. 204–211, 2015.
https://doi.org/10.1016/j.jcis.2014.09.064

[134] Cunha, D. L., Kuznetsov, A., Achete, C. A., da Hora Machado, A. E., Marques, M. "Immobilized TiO_2 on glass spheres applied to heterogeneous photocatalysis: photoactivity, leaching and regeneration process", PeerJ, 6, Article number: e4464, 2018.
https://doi.org/10.7717/peerj.4464

[135] Badvi, K., Javanbakht, V. "Enhanced photocatalytic degradation of dye contaminants with TiO_2 immobilized on ZSM-5 zeolite modified with nickel nanoparticles", Journal of Cleaner Production, 280(2), Article number: 124518, 2021.
https://doi.org/10.1016/j.jclepro.2020.124518

[136] Alias, S. S., Harun, Z., Azhar, F. H., Ibrahim, S. A., Johar, B. "Comparison between commercial and synthesised nano flower-like rutile TiO_2 immobilised on green super adsorbent towards dye wastewater treatment", Journal of Cleaner Production, 251, Article number: 119448, 2020.
https://doi.org/10.1016/j.jclepro.2019.119448

[137] Shao, L., Liu, H., Zeng, W., Zhou, C., Li, D., Wang, L., Lan, Y., Xu, F., Liu, G. "Immobilized and photocatalytic performances of PDMS-SiO_2-chitosan@TiO_2 composites on pumice under simulated sunlight irradiation", Apllied Surface Science, 478, pp. 1017–1026, 2019.
https://doi.org/10.1016/j.apsusc.2019.02.060

[138] Castañeda-Contreras, J., Marañón-Ruiz, V. F., Chiu-Zárate, R., Pérez-Ladrón De Guevara, H., Rodriguez, R., Michel-Uribe, C. "Photocatalytic activity of erbium-doped TiO_2 nanoparticles immobilized in macro-porous silica films", Materials Research Bulletin, 47(2), pp. 290–295, 2012.
https://doi.org/10.1016/j.materresbull.2011.11.021

[139] Saiful Amran, S. N. B., Wongso, V., Abdul Halim, N. S., Husni, M. K., Sambudi, N. S., Wirzal, M. D. H. "Immobilized carbon-doped TiO_2 in polyamide fibers for the degradation of methylene blue", Journal Of Asian Ceramic Societies, 7(3), pp. 321–330, 2019.
https://doi.org/10.1080/21870764.2019.1636929

[140] Nawawi, W. I., Zaharudin, R., Ishak, M. A. M., Ismail, K., Zuliahani, A. "The Preparation and Characterization of Immobilized TiO_2/PEG by Using DSAT as a Support Binder", Applied Sciences, 7(1), Article number: 24, 2017.
https://doi.org/10.3390/app7010024

[141] Chen, C., Ma, Z., Zhou, S., Li, T., Sun, X. "Cobalt-Tetracarboxyl-Phthalocyanine Linked with Fe_3O_4/Chitosan Microsphereas—Efficient Catalyst for Dye Degradation", Catalysis Letters, 147(9), pp. 2399–2409, 2017.
https://doi.org/10.1007/s10562-017-2149-7

[142] Ramasundaram, S., Seid, M. G., Kim, H. E., Son, A., Lee, C., Kim, E. J., Hong, S. W. "Binder-free immobilization of TiO_2 photocatalyst on steel mesh via electrospraying and hot-pressing and its application for organic micropollutant removal and disinfection", Journal of Hazardous Materials, 360, pp. 62–70, 2018.
https://doi.org/10.1016/j.jhazmat.2018.07.100

[143] Teixeira, S., Martins, P. M., Lanceros-Méndez, S., Kühn, K., Cuniberti, G. "Reusability of photocatalytic TiO_2 and ZnO nanoparticles immobilized in poly(vinylidene difluoride)-co-trifluoroethylene", Applied Surface Science, 384, pp. 497–504, 2016.
https://doi.org/10.1016/j.apsusc.2016.05.073

[144] Sutisna, Rokhmat, M., Wibowo, E., Murniati, R., Khairurrijal, Abdullah, M. "Application of Immobilized Titanium Dioxide as Reusable Photocatalyst on Photocatalytic Degradation of Methylene Blue", Advanced Materials Research, 1112, pp. 149–153, 2015.
https://doi.org/10.4028/www.scientific.net/amr.1112.149

[145] Belayachi, H., Bestani, B., Benderdouche, N., Belhakem, M. "The use of TiO_2 immobilized into grape marc-based activated carbon for RB-5 Azo dye photocatalytic degradation", Arabian Journal of Chemistry, 12(8), pp. 3018–3027, 2019.
https://doi.org/10.1016/j.arabjc.2015.06.040

[146] Ribeiro, L. N., Fonseca, A. C. S., da Silva, E. F. M., Oliveira, E. D. C., Ribeiro, A. T. S., Maranhão, L. C. A., Pacheco, J. G. A., Machado, G., Almeida, L. C. "Residue-based TiO_2/PET photocatalytic films for the degradation of textile dyes: A step in the development of green monolith reactors", Chemical Engineering and Processing - Process Intensification, 147, Article number: 107792, 2020.
https://doi.org/10.1016/j.cep.2019.107792

[147] Khaledi Maki, L., Maleki, A., Rezaee, R., Daraei, H., Yetilmezsoy, K. "LED-activated immobilized Fe-Ce-N tri-doped TiO_2 nanocatalyst on glass bed for photocatalytic degradation organic dye from aqueous solutions", Environmental Technology & Innovation, 15, Article number: 100411, 2019.
https://doi.org/10.1016/j.eti.2019.100411

[148] Behpour, M., Shirazi, P., Rahbar, M. "Immobilization of the Fe_2O_3/TiO_2 photocatalyst on carbon fiber cloth for the degradation of a textile dye under visible light irradiation", Reaction Kinetics, Mechanisms and Catalysis, 127(2), pp. 1073–1085, 2019.
https://doi.org/10.1007/s11144-019-01581-1

[149] González-Casamachin, D. A., Rivera De la Rosa, J., Lucio-Ortiz, C. J., De Haro De Rio, D. A., Martínez-Vargas, D. X., Flores-Escamilla, G. A., Dávila Guzman, N. E., Ovando-Medina, V. M., Moctezuma-Velazquez, E. "Visible-light photocatalytic degradation of acid violet 7 dye in a continuous annular reactor using ZnO/PPy photocatalyst: Synthesis, characterization, mass transfer effect evaluation and kinetic analysis", Chemical Engineering Journal, 373, pp. 325–337, 2019.
https://doi.org/10.1016/j.cej.2019.05.032

[150] Liji Sobhana, S. S., Mehedi, R., Malmivirta, M., Paturi, P., Lastusaari, M., Dîrtu, M. M., Garcia, Y., Fardim, P. "Heteronuclear nanoparticles supported hydrotalcites containing Ni(II) and Fe(III) stable photocatalysts for Orange II degradation", Applied Clay Science, 132–133, pp. 641–649, 2016.
https://doi.org/10.1016/j.clay.2016.08.016

[151] Lee, S. L., Ho, L. N., Ong, S. A., Wong, Y. S., Voon, C. H., Khalik, W. F., Yusoff, N. A., Nordin, N. "A highly efficient immobilized ZnO/Zn photoanode for degradation of azo dye Reactive Green 19 in a photocatalytic fuel cell", Chemosphere, 166, pp. 118–125, 2017.
https://doi.org/10.1016/j.chemosphere.2016.09.082

[152] Akerdi, A. G., Bahrami, S. H., Arami, M., Pajootan, E. "Photocatalytic discoloration of Acid Red 14 aqueous solution using titania nanoparticles immobilized on graphene oxide fabricated plate", Chemosphere, 159, pp. 293–299, 2016.
https://doi.org/10.1016/j.chemosphere.2016.06.020

[153] Kim, C., Kim, J. T., Kim, K. S., Jeong, S., Kim, H. Y., Han, Y. S. "Immobilization of TiO_2 on an ITO substrate to facilitate the photoelectrochemical degradation of an organic dye pollutant", Electrochimical Acta, 54(24), pp. 5715–5720, 2009.
https://doi.org/10.1016/j.electacta.2009.05.018

[154] Yildiz, T., Yatmaz, H. C., Öztürk, K. "Anatase TiO_2 powder immobilized on reticulated Al_2O_3 ceramics as a photocatalyst for degradation of RO16 azo dye", Ceramics International, 46(7), pp. 8651–8657, 2020.
https://doi.org/10.1016/j.ceramint.2019.12.098

[155] Ghoreishian, S. M., Badii, K., Norouzi, M., Malek, K. "Effect of cold plasma pre-treatment on photocatalytic activity of 3D fabric loaded with nano-photocatalysts: Response surface methodology", Applied Surface Science, 365, pp. 252–262, 2016.
https://doi.org/10.1016/j.apsusc.2015.12.155

[156] Nawi, M. A., Sabar, S., Sheilatina "Photocatalytic decolourisation of Reactive Red 4 dye by an immobilised TiO_2/chitosan layer by layer system", Journal of Colloid Interface Science, 372(1), pp. 80–87, 2012.
https://doi.org/10.1016/j.jcis.2012.01.024

[157] Wan Ismail, W. I. N., Ain, S. K., Zaharudin, R., Jawad, A. H., Ishak, M. A. M., Ismail, K., Sahid, S. "New TiO_2/DSAT Immobilization System for Photodegradation of Anionic and Cationic Dyes", International Journal of Photoenergy, 2015, Article ID: 232741, 2015.
https://doi.org/10.1155/2015/232741

[158] Baudys, M., Zlámal, M., Krýsa, J., Jirkovský, J., Kluson, P. "Notes on heterogeneous photocatalysis with the model azo dye acid orange 7 on TiO_2", Reaction Kinetics, Mechanisms and Catalysis, 106(2), pp. 297–311, 2012.
https://doi.org/10.1007/s11144-012-0438-0

[159] Adamek, E., Baran, W., Ziemiańska-Błaszczyk, J., Sobczak, A. "Immobilisation of TiO_2-P25 on a glass fibre mat: Preparation, photocatalytic activity and stability", Solar Energy, 188, pp. 1232–1242, 2019.
https://doi.org/10.1016/j.solener.2019.07.034

[160] Qourzal, S., Barka, N., Tamimi, M., Assabbane, A., Ait-Ichou, Y. "Photodegradation of 2-naphthol in water by artificial light illumination using TiO_2 photocatalyst: Identification of intermediates and the reaction pathway", Applied Catalysis A: General, 334(1–2), pp. 386–393, 2008.
https://doi.org/10.1016/j.apcata.2007.09.034

[161] Jyothi, K. P., Yesodharan, S., Yesodharan, E. P. "Ultrasound (US), Ultraviolet light (UV) and combination (US + UV) assisted semiconductor catalysed degradation of organic pollutants in water: Oscillation in the concentration of hydrogen peroxide formed in situ", Ultrasonic Sonochemistry, 21(5), pp. 1787–1796, 2014.
https://doi.org/10.1016/j.ultsonch.2014.03.019

[162] Mozia, S. "Photocatalytic membrane reactors (PMRs) in water and wastewater treatment. A review", Separation and Purification Technology, 73(2), pp. 71–91, 2010.
https://doi.org/10.1016/j.seppur.2010.03.021

[163] Paz, Y. "Preferential photodegradation - why and how?", Comptes Rendus Chimie, 9(5–6), pp. 774–787, 2006.
https://doi.org/10.1016/j.crci.2005.03.032

[164] Herrmann, J. M. "Heterogeneous photocatalysis: state of the art and present applications In honor of Pr. R.L. Burwell Jr. (1912–2003), Former Head of Ipatieff Laboratories, Northwestern University, Evanston (Ill).", Topics in Catalysis, 34(1), pp. 49–65, 2005.
https://doi.org/10.1007/s11244-005-3788-2

[165] Herrmann, J. M. "Heterogeneous photocatalysis: fundamentals and applications to the removal of various types of aqueous pollutants", Catalysis Today, 53(1), pp. 115–129, 1999.
https://doi.org/10.1016/S0920-5861(99)00107-8

[166] Neppolian, B., Choi, H. C., Sakthivel, S., Arabindoo, B., Murugesan, V. "Solar light induced and TiO_2 assisted degradation of textile dye reactive blue 4", Chemosphere, 46(8), pp. 1173–1181, 2002.
https://doi.org/10.1016/S0045-6535(01)00284-3

[167] Konstantinou, I. K., Albanis, T. A. "TiO_2-assisted photocatalytic degradation of azo dyes in aqueous solution: kinetic and mechanistic investigations: A review", Applied Catalysis B: Environmental, 49(1), pp. 1–14, 2004.
https://doi.org/10.1016/j.apcatb.2003.11.010

[168] Daneshvar, N., Salari, D., Khataee, A. R. "Photocatalytic degradation of azo dye acid red 14 in water: investigation of the effect of operational parameters", Journal of Photochemistry and Photobiology A: Chemistry, 157(1), pp. 111–116, 2003.
https://doi.org/10.1016/S1010-6030(03)00015-7

[169] Ling, H., Kim, K., Liu, Z., Shi, J., Zhu, X. Huang, J. "Photocatalytic degradation of phenol in water on as-prepared and surface modified TiO_2 nanoparticles", Catalysis Today, 258(1), pp. 96–102, 2015.
https://doi.org/10.1016/j.cattod.2015.03.048

[170] Valente, J. P. S., Padilha, P. M., Florentino, A. O. "Studies on the adsorption and kinetics of photodegradation of a model compound for heterogeneous photocatalysis onto TiO_2", Chemosphere, 64(7), pp. 1128–1133, 2006.
https://doi.org/10.1016/j.chemosphere.2005.11.050

[171] Chiou, C. H., Wu, C. Y., Juang, R. S. "Influence of operating parameters on photocatalytic degradation of phenol in UV/TiO_2 process", Chemical Engineering Journal, 139(2), pp. 322–329, 2008.
https://doi.org/10.1016/j.cej.2007.08.002

[172] Ollis, D. F., Pelizzetti, E., Serpone, N. "Photocatalyzed destruction of water contaminants", Environmental Science & Technology, 25(9), pp. 1522–1529, 1991.
https://doi.org/10.1021/es00021a001

[173] Ahmad, R., Ahmad, Z., Khan, A. U., Mastoi, N. R., Aslam, M., Kim, J. "Photocatalytic systems as an advanced environmental remediation: Recent developments, limitations and new avenues for applications", Journal of Environmental Chemical. Engineering. 4(4), pp. 4143–4164, 2016.
http://doi.org/10.1016/j.jece.2016.09.009